



Apatite (U–Th)/He thermochronology and Re–Os ages in the Altar region, Central Andes (31°30'S), Main Cordillera of San Juan, Argentina: implications of rapid exhumation in the porphyry Cu (Au) metal endowment and regional tectonics

Laura Maydagán^{1,2} · Massimiliano Zattin³ · Constantino Mpodozis⁴ · David Selby^{5,6} · Marta Franchini^{1,7} · Luis Dimieri²

Received: 25 February 2019 / Accepted: 26 November 2019
© Springer-Verlag GmbH Germany, part of Springer Nature 2020

Abstract

Altar is a large porphyry Cu (Au) deposit located in the Main Cordillera of Argentina, 20 km to the north of the giant Los Pelambres–El Pachón porphyry copper cluster, at the southern portion of the Pampean flat-slab segment of the Andes. Although this region hosts telescoped porphyry-epithermal deposits, the precise temporal relationship between porphyry emplacement, mineralization, cooling, and regional orogenic uplift are still poorly understood. New Re–Os molybdenite ages indicate that Altar orebodies are associated with two magmatic hydrothermal centers: Altar East (11.16 ± 0.06 Ma) and Altar Central (10.38 ± 0.05 Ma) formed at temporally distinct periods. New (U–Th)/He ages from the Early Permian and Late Eocene plutons, and the Middle Miocene subvolcanic stocks associated with Cu–Au mineralization of the Altar region reflect a rapid cooling pulse during the Middle Miocene (15.02 to 10.66 Ma) coeval with a major phase of tectonic shortening and regional uplift. The main pulse of rapid cooling and related tectonic uplift in the Altar region was synchronous with the formation of the hydrothermal systems and resulted in an increased focused metal endowment (Au–Cu grades) due to the telescoping of epithermal mineralization over the rapidly uplifted porphyry system. This 11–10 Ma tectonically triggered exhumation event coincides with the collision of the E-trending segment of the Juan Fernández Ridge with the Peru–Chile trench, at this latitude. Collision and ensuing ridge subduction may have driven a localized pulse of rapid cooling and exhumation of the Main Cordillera that has not been well documented to the north or south of the Altar–Los Pelambres region.

Keywords U–Th/He in apatite · Andes · Miocene · Re–Os in molybdenite · Exhumation · Argentina

Editorial handling: P. Hollings

Electronic supplementary material The online version of this article (<https://doi.org/10.1007/s00126-019-00946-9>) contains supplementary material, which is available to authorized users.

✉ Laura Maydagán
lauramaydagan@yahoo.com.ar

¹ CONICET, Centro Patagónico de Estudios Metalogenéticos, Buenos Aires, Argentina

² INGEOSUR–CONICET, Departamento de Geología, Universidad Nacional del Sur, San Juan 670, 8000 Bahía Blanca, Argentina

³ Department of Geosciences, University of Padua, Via G. Gradenigo 6, 35131 Padova, Italy

⁴ Antofagasta Minerals, Apoquindo 4001, Piso 18, Santiago, Chile

⁵ Department of Earth Sciences, University of Durham, Durham DH1 3LE, UK

⁶ State Key Laboratory of Geological Processes and Mineral Resources, School of Earth Resources, China University of Geosciences, Wuhan, China

⁷ Departamento de Geología y Petróleo, Facultad de Ingeniería, Universidad Nacional del Comahue, Buenos Aires 1400, 8300 Neuquén, Argentina

Introduction

Altar is a large porphyry Cu (Au) deposit with associated high sulfidation epithermal veins (measured and indicated resources of 2 Gt at 0.34% copper and 0.1 g/t gold; Aldebaran Resources 2018), located in the Cordillera Principal of San Juan Province, Argentina, near the Argentina–Chile border. The deposit occurs at the southern portion of the modern Pampean flat-slab segment (Cahill and Isacks 1992; Kay and Mpodozis 2002; Anderson et al. 2007; Ammirati et al. 2016; Haddon and Porter 2018, Fig. 1) and forms part of the southern Central Andes Miocene–Pliocene porphyry copper belt that, in Chile, hosts three of the largest copper deposits in the world (El Teniente, 75 Mt Cu; Río Blanco–Los Bronces, 204 Mt Cu; Los Pelambres–El Pachón, 21 Mt Cu; Cooke et al. 2005; Sillitoe and Perelló 2005; Irarrazaval et al. 2010, Fig. 2). Numerous Cu (Au) prospects with high mining potential have been recently discovered in the area, some exhibiting telescoped porphyry type and high sulfidation epithermal systems. These telescoped systems are interpreted to reflect synmineral erosion, progressive paleosurface lowering, and alteration-mineralization overlapping as a result of compressive deformation and uplift (e.g., Sillitoe 1994; Sillitoe et al. 2019).

The Altar deposit represents an environment that transitions from the basal roots of a high sulfidation epithermal lithocap to a sub-volcanic porphyry copper environment at depth. The deposit is described as telescoped because of the close spatial distance between the porphyry and the high sulfidation alteration systems (Aldebaran Resources 2018). Metallic mineralization at the Altar Central orebody occurred through successive stages of vein formation: (1) quartz ± chalcopyrite ± pyrite veins (A veins) and (2) quartz ± molybdenite veins (B veins), both formed during early potassic alteration at high temperature and pressures, and (3) late-stage veins rich in Cu sulfides and sulfosalts (E veins) that formed at low temperatures equivalent or transitional to the epithermal environment, and cross-cut the early veins (Maydagán et al. 2015). The epithermal veins are considered to be slightly younger than the porphyry veins implying that the hydrothermal system would have developed in an active tectonic environment.

In this study, we present new Re–Os molybdenite data to better constrain the timing of Altar mineralization, and new apatite (U–Th)/He data in order to investigate the low-temperature cooling history of igneous and sedimentary rocks of the region. We analyze the causes of cooling and discuss whether the cooling events related to the tectonic pulses could affect the presence and grade of porphyry-epithermal mineral deposits. We compare our results with the tectonic/uplift history of the Coastal, Main, and Frontal Cordilleras at this latitude, and with previous studies in other areas of the modern Pampean flat-slab region.

Tectonic setting

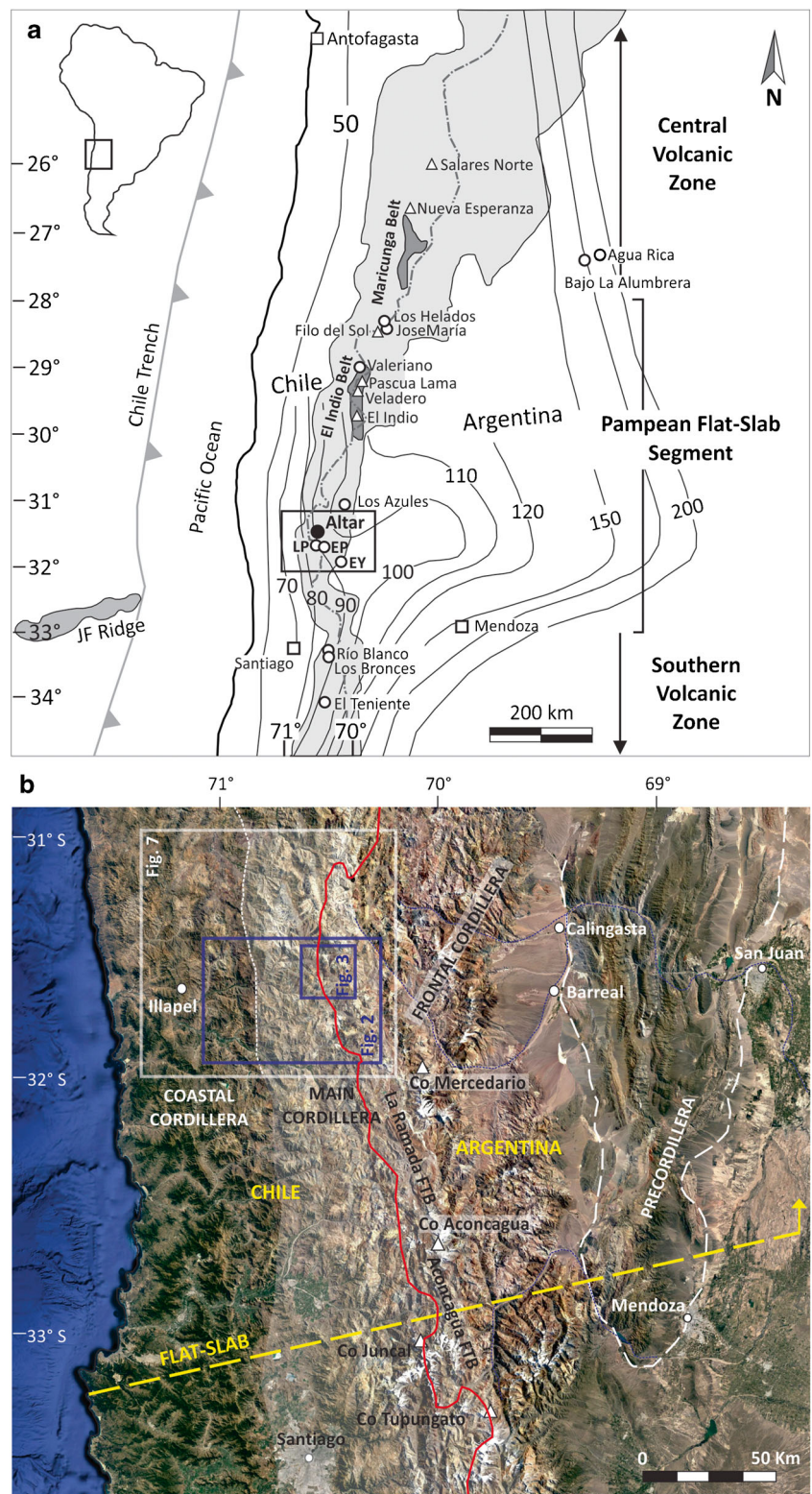
The Altar deposit is located in the present-day amagmatic Pampean flat-slab segment of the central Argentina and Chile, which hosts two of the three largest known porphyry copper–molybdenum deposits of Central Chile: Río Blanco–Los Bronces and Los Pelambres–El Pachón (Cooke et al. 2005; Sillitoe and Perelló 2005; Irarrazaval et al. 2010; Fig. 1). This metallogenic belt was constructed atop the Chilenia Terrane, a microcontinental block accreted to the Gondwana margin in the Devonian (Ramos et al. 1986) that was later the site of subduction-related arc-magmatism during the Pennsylvanian to early Permian (Mpodozis and Kay 1992), rifting and extension-related magmatism during the Middle Permian to Triassic (Sato et al. 2015), marine sedimentation in a backarc setting (Neuquén Basin) during the Jurassic–Early Cretaceous (Cristallini and Ramos 2000), and subduction-related calc-alkaline volcanism and associated plutonism during the Cretaceous through the Cenozoic (Mpodozis and Ramos 1989). During the Oligocene and Early Miocene, thick volcano-sedimentary sequences accumulated in an extensional volcano-tectonic basin or intra-arc depression (Abanico/Coya Machalí Basin, Jordan et al. 2001; Charrier et al. 2002, 2005). Compressional deformation and basin collapse began in the Early Miocene at ca. 20–18 Ma, coinciding with the initiation of the oceanic Nazca slab shallowing (Kay and Mpodozis 2002).

Geology of the Los Pelambres–Altar region (31°–32°S)

The geology of the Altar–Los Pelambres region is characterized by four structural domains that show different stratigraphy and structural style and are bounded by N-trending, high-angle reverse faults.

The easternmost Domain 1 encompasses a westward-tilted block including granites and silicic volcanic rocks assigned to the Permo-Triassic Choiyoi Group (Alvarez 1996; Cristallini and Ramos 2000) that form the highest peaks of the Cordillera Santa Cruz (Fig. 2). This block is thrust toward the east, on top of the major high angle, west dipping reverse, Santa Cruz Fault, over Miocene synorogenic (< 18 Ma) red conglomerate and sandstone sequences (Cristallini and Ramos 2000). To the west the Choiyoi Group is unconformably covered by Late Triassic rift (ca. 200 Ma) deposits (Rancho de Lata Formation, Alvarez 1996; Mackaman-Lofland et al. 2019) and a thin sequence of Jurassic to Cretaceous marine and continental sedimentary strata that include the northernmost known outcrops of the Neuquén backarc basin infill (Alvarez 1996; Cristallini and Ramos 2000). These Mesozoic sedimentary rocks are, in turn, unconformably covered by continental volcanoclastic conglomerate and breccia, rhyolitic tuff, and pyroxene–hornblende bearing andesite and dacite, grouped as the Mondaca Strata, which yielded LA-ICPMS U–Pb zircon ages

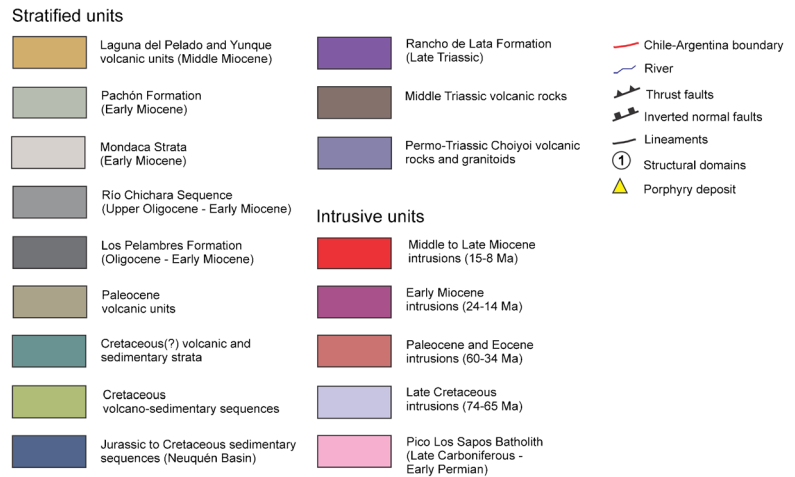
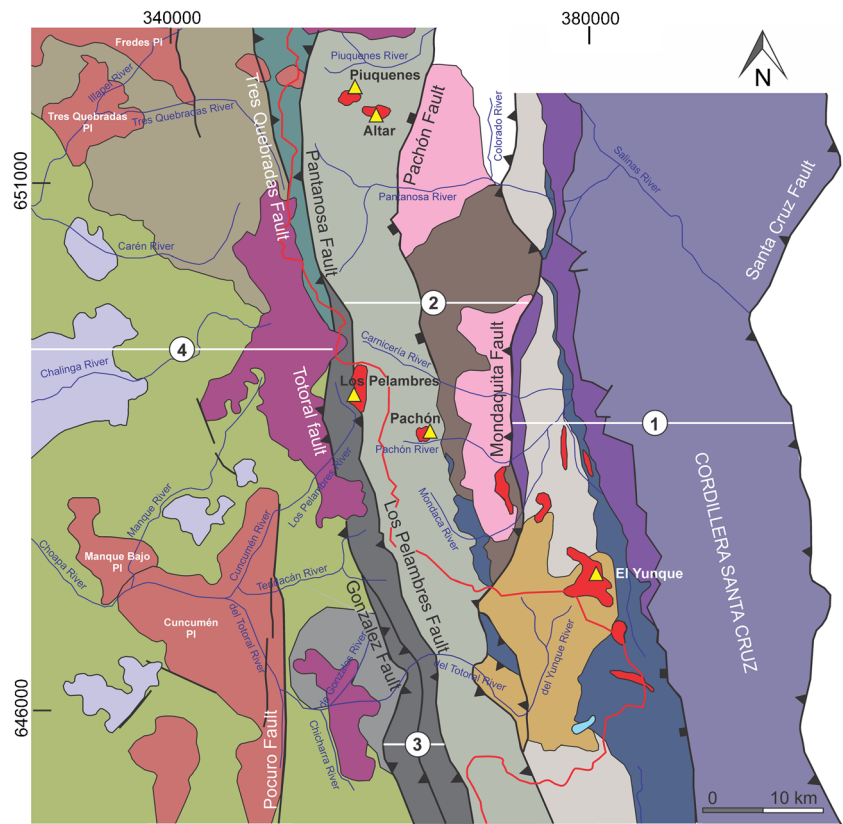
Fig. 1 **a** Location of the study area (rectangle) in the Pampean Flat-Slab segment relative to depth contours on the Wadati–Benioff zone (Cahill and Isacks 1992; Anderson et al. 2007). Note the actual position of the Juan Fernández Ridge (Yáñez et al. 2001), the Central Volcanic Zone, and the Southern Volcanic Zone. Metallogenic belts (dark gray), porphyry-type deposits (circles), and high sulfidation epithermal deposits (triangles) are shown. Abbreviations: EP: El Pachón deposit, EY: El Yunque deposit, JF: Juan Fernández, LP: Los Pelambres deposit. **b** Morphostructural units of the Andes between 31°S and 34°S: Coastal Cordillera, Main Cordillera (Cordillera Principal), Frontal Cordillera, La Ramada and Aconcagua fold and thrust belts, Precordillera, and Sierra de Pie de Palo. Location of Figs. 2, 3, and 7 are shown



between 22.1 ± 0.4 and 21.6 ± 0.4 Ma (Mpodozis et al. 2009, Fig. 2). To the south, 20° – 30° W dipping rocks of this unit are covered, in angular unconformity, by gently dipping to subhorizontal Lower Miocene volcanic rocks with LA-

ICPMS U–Pb ages between 20 and 14 Ma (Laguna del Pelado and Yunque volcanic complexes, Mpodozis et al. 2009, Fig. 2), which provides evidence of a regional compressive deformation event at ~ 20 Ma. Middle to Late Miocene

Fig. 2 Geological map of the study region between 31°S and 32°S based on Mpodozis (2016). Location of structural domains described in the text, main faults, and mineral deposits



intrusions in this domain are linked to porphyry-type deposits (e.g., El Yunque, Fig. 2).

Domain 2 is bounded by another east-verging reverse fault (Mondaquita Fault) that brings “basement” late Paleozoic–Triassic rocks on top of the Mondaca Strata and/or the Laguna del Pelado Volcanic Complex (Fig. 2). The oldest rocks of this domain include small and isolated outcrops of clastic metasedimentary rocks (Alfarcillo Metamorphic Complex, Musso et al. 2012) and undated

silicic volcanic rocks intruded by Late Carboniferous to Early Permian granitoids of the Pico Los Sapos batholith (Mpodozis et al. 1976) that includes 297 ± 4 Ma tonalite (zircon LA-ICPMS U–Pb age, Maydagán 2012) and granite dated at 301.4 ± 2.3 Ma by the same method (Musso et al. 2012). The Paleozoic rocks are capped, between Río Carnicería and Río Pantanosa, by a sequence of around 500 m of rhyolitic lavas and pyroclastic rocks which yielded a Middle Triassic LA-ICPMS U–Pb zircon age

(ca. 239 Ma, Mpodozis et al. 2009; Mpodozis 2016). The western area of Domain 2 is formed by regionally extensive outcrops of olivine-bearing basaltic to andesitic lava flows and rare felsic tuff of the Pachón Formation (Fernández et al. 1974; Lencinas and Tonel 1993) with U–Pb zircon ages between 22.7 ± 0.2 and 21.69 ± 0.26 Ma (Mpodozis et al. 2009; Perelló et al. 2012). Outcrops of the Pachón Formation are bounded to the east by the Pachón Fault (Fig. 2), a west dipping, partly inverted normal fault that brings the volcanic rocks in contact with Late Paleozoic to Middle Triassic rocks (Mpodozis et al. 2009).

Rocks belonging to the Pachón Formation host the late Miocene subvolcanic porphyry intrusions associated with the El Pachón (Fernández et al. 1974), Piuquenes, and Altar porphyry copper systems (Fig. 2). At Altar, they include a lower unit of basaltic andesite and porphyritic andesite–dacite lavas, andesitic–dacitic lapilli tuff, and pyroclastic breccia that grade upwards to a unit of compact and thick rhyolitic tuff (U–Pb zircon ages of 21.6 ± 1.2 Ma and 20.8 ± 0.3 Ma, Maydagán et al. 2011; Maydagán 2012). Both the Pachón Formation and the Mondaca Strata are, in part, equivalent to the regionally extensive volcanic Abanico/Coya-Machalí formations that form the bulk of the main Cordillera of Central Chile (33° – 36° S, Aguirre 1960; Klohn 1960; Thiele 1980; Charrier et al. 2002; Piquer et al. 2017).

Domain 3 is a narrow 5-km-wide, N-trending ribbon of strongly deformed volcanic and sedimentary rocks straddling the Argentina–Chile border and bounded to the east by the high angle, reverse, E-verging Los Pelambres–Pantanosá Fault System, and to the west by the W-verging Totoral–Tres Quebradas faults (Fig. 2). Near the Los Pelambres deposit, Domain 3 comprises a sequence of andesitic to basaltic lava flows, tuff, and local lacustrine ostracod-bearing limestone (Los Pelambres Formation), first described by Rivano and Sepúlveda (1991) who attributed this unit to the early Cretaceous. Several LA-ICPMS U–Pb zircon ages ranging from 33.4 to 18.0 Ma confirm, however, its Early Oligocene to Early Miocene age (Mpodozis et al. 2009; Perelló et al. 2012). This unit is intensely deformed as indicated by vertical and overturned strata, anastomosing, thrust-bounded tectonic lenses, and widespread mesoscale, sub-isoclinal folds (Mpodozis et al. 2009; Mpodozis 2016). The high strain Domain 3 can be traced northward into the Altar region, bordered by the La Pantanosá and Tres Quebradas faults where a sequence of continental red beds and andesitic to basaltic lavas, not yet dated, but likely of Cretaceous age (Fig. 2), are intruded by the Late Eocene del Medio Pluton (Mpodozis 2016, Fig. 3).

Middle to Late Miocene intrusions (14–8 Ma) related to the mineralized systems of Los Pelambres, Pachón, Piuquenes, and Altar, representing the last episodes of magmatic activity in the region, outcrop in Domains 2 and 3 (Fig. 2). In the Los Pelambres porphyry deposit, the post-kinematic and pre-mineral Los Pelambres stock, which was emplaced along the trace of Los Pelambres Fault at the boundary between Domains 2 and 3 (Fig. 2), yielded LA-ICPMS U–Pb ages of 13.92 ± 0.15 and 13.00 ± 0.7 Ma (Bertens et al. 2003, 2006; Perelló et al. 2012). The Los Pelambres–Frontera cluster of Cu–Mo mineralized porphyries, which intrude both the precursor stock and the Pachón Formation of Domain 2, have LA-ICPMS U–Pb zircon crystallization ages between 12.3 and 10.5 Ma (Perelló et al. 2012). By comparison, the intrusive suite hosting the majority of Cu–Au mineralization at Altar comprises a series of porphyritic intrusions, dykes, and magmatic-hydrothermal breccias emplaced in the Pachón Formation, but no early large precursor stock as in Los Pelambres has been found (Maydagán et al. 2014, Fig. 3).

Altar hosts three main porphyry copper–gold mineralization centers: Altar East, Altar Central, and the recently discovered Quebrada de la Mina–Radio, 3 km to the west of Altar Central. Zircon LA-ICPMS U–Pb ages from the Altar East and Altar Central orebodies indicate the occurrence of four discrete intrusive events over a period of ca. 3 m.y. The intrusions comprise a pre-mineralization porphyry (porphyry 1, 11.75 ± 0.24 Ma), three mineralized porphyries related to hydrothermal breccias (porphyry 2, 11.62 ± 0.21 and 11.68 ± 0.27 Ma; porphyry 3, 11.13 ± 0.26 Ma; porphyry 4, 10.35 ± 0.32 Ma), and two post-mineralization intrusions along with a post-mineralization intrusive breccia (8.9 ± 0.4 Ma, Maydagán et al. 2011, 2014, Fig. 3). Altar is noteworthy for having relatively higher gold grades associated with copper mineralization, at an average Au/Cu ratio of 0.14×10^{-4} for the Altar Central orebody (Zwahlen et al. 2014), compared to the nearby giant Chilean deposits such as Los Bronces and Los Pelambres (Mutschler et al. 2010).

The westernmost Domain 4 in Chile west of the Totoral–González and Tres Quebradas faults is, by contrast, characterized by a >2-km-thick, unfolded, gently E-dipping sequence of Middle to Late Cretaceous sedimentary and volcanic strata (from base to top—Quebrada Marquesa Formation, Salamanca Formation, and Almendrillo Strata) which, at this latitude, form the youngest Mesozoic stratified sequences of the Chilean Coastal Range (Rivano and Sepúlveda 1991; Mpodozis et al. 2009; Bergoing 2016, Fig. 2). North of Los Pelambres, an Early Paleocene volcanic sequence rests on top of the Almendrillo Strata (75–70 Ma) while, to the south, the

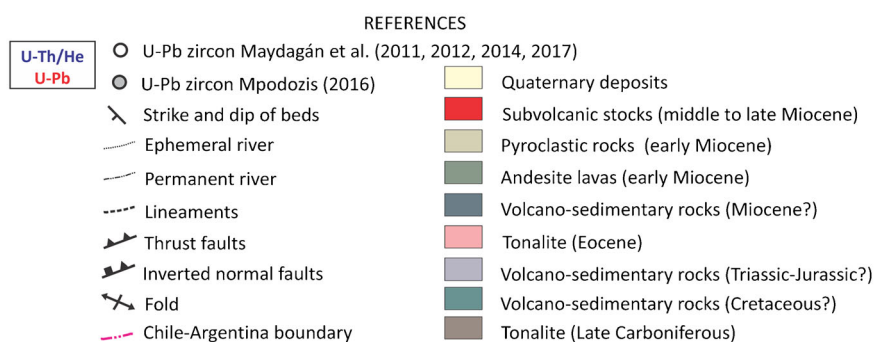
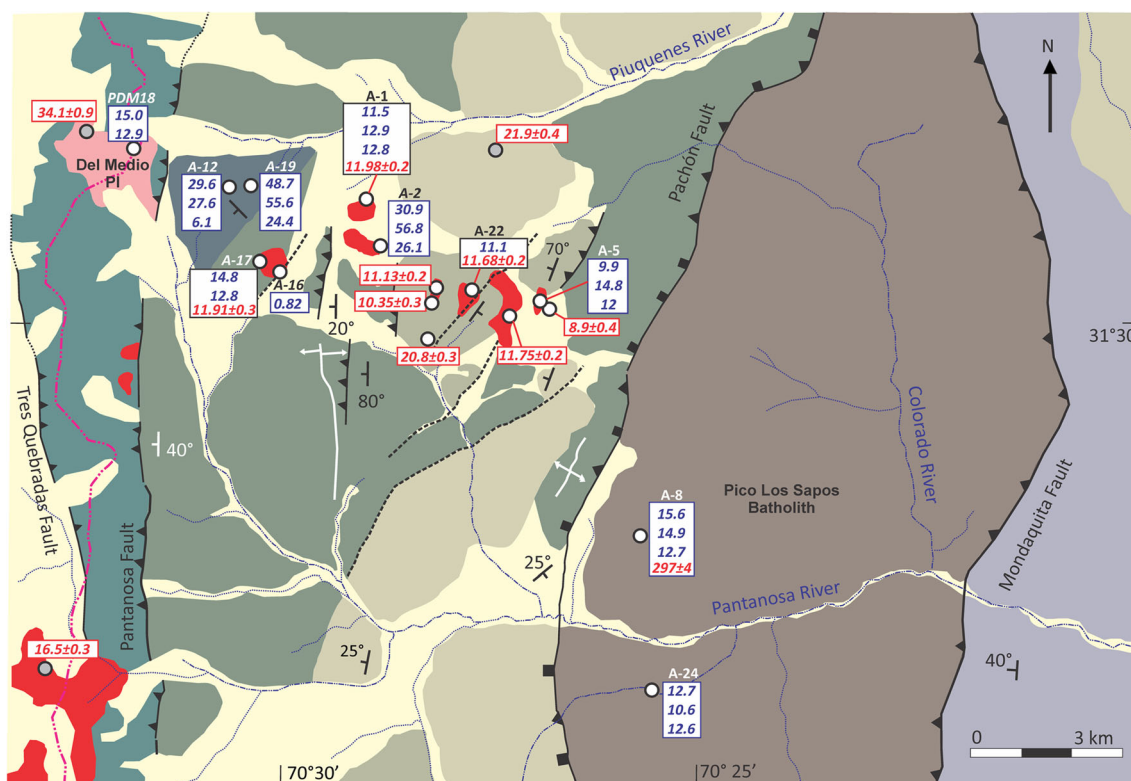


Fig. 3 Geologic map of the Altar District showing the location of U–Pb ages from Maydagán et al. (2011, 2012, 2014, 2017) and Mpodozis (2016) and the new U–Th/He ages (this study)

Cretaceous rocks are covered through a remarkable angular unconformity by a Late Oligocene to Early Miocene volcanic sequence (Río Chicharra Strata, Fig. 2). Late Cretaceous, Paleocene, Eocene, Oligocene, and Early to Middle Miocene plutons and stocks, of generally intermediate composition, intrude the volcanic and volcano-sedimentary sequences of Domain 4 (Fig. 2).

Methodology

A suite of samples was collected from the Altar region to carry out geochronological analysis by Re–Os in molybdenite and (U–Th)/He in apatite (ESM 1).

Two molybdenite samples, obtained from the drill-holes of the Altar Central and Altar East deposits, were analyzed in the Source Rock and Sulfide Geochemistry and Geochronology, and Arthur Holmes Laboratories at University of Durham (UK) to establish the Re–Os age of molybdenite mineralization (ESM 1). Samples of B veins rich in molybdenite were selected from the Altar East deposit (drill hole ALD-178, depth 153 m) and the Altar Central deposit (drill hole ALD-68, depth 440 m). Molybdenite separation was achieved through using traditional methods (crushing to 70 to 200 mesh, magnetic separation, heavy liquids, and final hand picking to remove any impurities). An aliquant of the molybdenite separate (~20 mg) together with a known amount of

tracer solution ($^{185}\text{Re} + \text{Os}$ bearing a normal isotope composition) were placed into a carius tube and digested with 3 mL HCl and 6 mL HNO_3 at 220 °C for 23 h. Osmium was isolated and purified using solvent extraction (CHCl_3) and microdistillation methods, with the resulting Re-bearing fraction purified using NaOH–acetone solvent extraction and anion chromatography (Selby and Creaser 2004; Li et al. 2017). Although negligible in comparison to the Re and Os abundance in the molybdenite, the final Re–Os data are blank corrected. A full analytical protocol blank run parallel with the molybdenite analysis yields 3.2 pg Re and 0.8 pg Os, the latter possessing a $^{187}\text{Os}/^{188}\text{Os}$ composition of 0.21 ± 0.2 . See Li et al. (2017) regarding data treatment, standards, and reference materials.

Two samples for U–Th/He analysis were obtained from the Late Carboniferous–Early Permian tonalites of the Pico Los Sapos batholith (Samples A24 and A8, Fig. 3). One sample was obtained from the Late Eocene del Medio Pluton (Fig. 3). Two samples were taken from a volcanic-sedimentary unit (Chinchimoye sequence), considered to be of Miocene age that crops out north of Quebrada de la Mina-Radio deposit (A12 and A19), and six samples (A1, A2, A5, A16, A17, A22) were taken from the Middle–Late Miocene porphyry intrusions (Fig. 3).

The mineral separates of the apatite crystals for U–Th/He analysis was carried out in both the laboratories of the Universidad Nacional del Sur (Argentina) and the University of Padova (Italy). The (U–Th)/He single grain ages were obtained from selected apatite grains (euhedral shape, overall size greater than 60 μm and without inclusions) at the University of Arizona, Tucson (USA). Sphere equivalent radius, weight, and ejection factors were determined assuming a homogeneous distribution of U and Th in apatite (Gautheron and Tassan-Got 2010; Gautheron et al. 2012). The apatite samples were placed in a niobium (Nb) basket and were heated twice using a diode laser at 1030 ± 50 °C for 5 min, allowing for total He degassing and to check the presence of He trapped in small inclusions (Fillon et al. 2013). After He extraction, the Nb baskets were placed into a single-use polypropylene vial. Apatite grains were dissolved for 3 h at 70 °C in 50 μL HNO_3 5 N solution containing a known content of

^{235}U , ^{230}Th , and ^{149}Sm , and additional 50 μL HNO_3 5 N and then filled with 0.9 mL of ultrapure MQ water. The final solution was measured for U, Th, and Sm concentrations by quadrupole inductively coupled plasma (ICP)-quadrupole mass spectrometry. The analysis was calibrated using external age standards, including Limberg Tuff and Durango apatites. The mean (U–Th)/He ages of the standards agree with published data (16.8 ± 1.1 Ma and 31.0 ± 1.0 ; McDowell et al. 2005; Kraml et al. 2006).

Results

Re–Os dates in molybdenite

Molybdenite from the Altar East deposit (drill hole ALD-178) contains 3546 ppm Re and 414 ppb ^{187}Os and yielded a Re–Os age of 11.16 ± 0.06 Ma, including analytical, tracer, and decay constant uncertainties. In comparison, the molybdenite from the Altar Central deposit (drill hole ALD-68) has lower Re (1868 ppm) and ^{187}Os (203 ppb), with a younger Re–Os age of 10.38 ± 0.05 Ma (Table 1, Figs. 4 and 5a).

U–Th/He dates in apatite

All apatite U–Th–He analytical data and weighted mean (U–Th)/He ages are presented in Table 2 and ESM 1. The Early Permian tonalite of the Pico Los Sapos Batholith (samples A-8 and A-24, Figs. 3 and 5b, c) yielded single grain (U–Th)/He ages between 15.69 and 10.66 Ma, with mean (U–Th)/He ages of 14.3 ± 0.29 Ma (number of grains = 3) and 11.87 ± 0.15 Ma ($n = 3$), respectively (Fig. 5b). The sample from the Late Eocene Plutón del Medio (PDM18), which crops out in the west sector of the Altar District (Figs. 3 and 5b, c), yielded single grain (U–Th)/He ages between 15.02 and 12.98 Ma, with a mean (U–Th)/He age of 13.46 ± 0.17 Ma ($n = 2$).

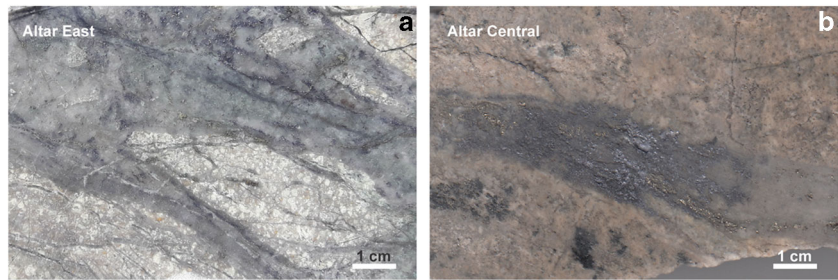
The two samples from the Miocene red sandstone and conglomerate of the Chinchimoye Sequence (A12 and A19) yielded individual (U–Th)/He grain ages of 29.63, 27.58, and 6.15 Ma, and 55.57, 46.60, and 24.44 Ma, respectively. Sample A-19 yield two grains older than their proposed Miocene age (Figs. 3 and 5b).

Table 1 Summary of the Re–Os data for the analyzed molybdenite samples

Sample	wt (g)	Re (ppm)	±	^{187}Re (ppm)	±	^{187}Os (ppb)	±	Age (Ma)	± ^a
ALD-178-153	0.020	3546.2	13.2	2228.9	8.3	414.4	1.32	11.16	0.06
A68-440	0.021	1867.6	6.9	1173.8	4.3	203.0	0.64	10.38	0.05

^aUncertainty including all sources of analytical uncertainty plus decay constant

Fig. 4 Samples of B-type veins from Altar East and Altar Central analyzed by Re–Os in molybdenite



The majority of the (U–Th)/He ages from the Middle to Late Miocene Altar subvolcanic stocks (70%) range between 14.87 and 9.96 Ma (Figs. 3 and 5b, c). Sample A-1 from the Altar North porphyry intrusion gave (U–Th)/He ages between 12.99 and 11.53 Ma, with a mean (U–Th)/He age of 12.18 ± 0.15 Ma. Sample A-2 (Altar North porphyry) exhibits (U–Th)/He ages older than the crystallization age of the intrusion

(56.83 Ma, 30.92 Ma, and 26.17 Ma, Table 2). Samples A-22 and A-5 from Altar East porphyry intrusions yielded (U–Th)/He ages between 14.87 and 9.96 Ma, and mean (U–Th)/He ages of 11.17 ± 0.4 Ma and 12.32 ± 0.26 Ma, respectively. Sample A-17 from a subvolcanic stock of Quebrada de la Mina deposit yielded (U–Th)/He ages between 14.87 and 12.8 Ma (mean (U–Th)/He age of 13.45 ± 0.27 Ma). Finally,

Fig. 5 **a** Summary of U–Pb ages from the Altar subvolcanic stocks from Maydagán et al. (2011, 2014, 2017) and the new Re–Os ages from Altar East and Altar Central. **b** Summary of U–Th/He ages from the study area. **c** Simplified west–east cross-section of the Altar District with location of the thermochronology samples relative to the main faults (Pantanosa Fault and Pachón Fault)

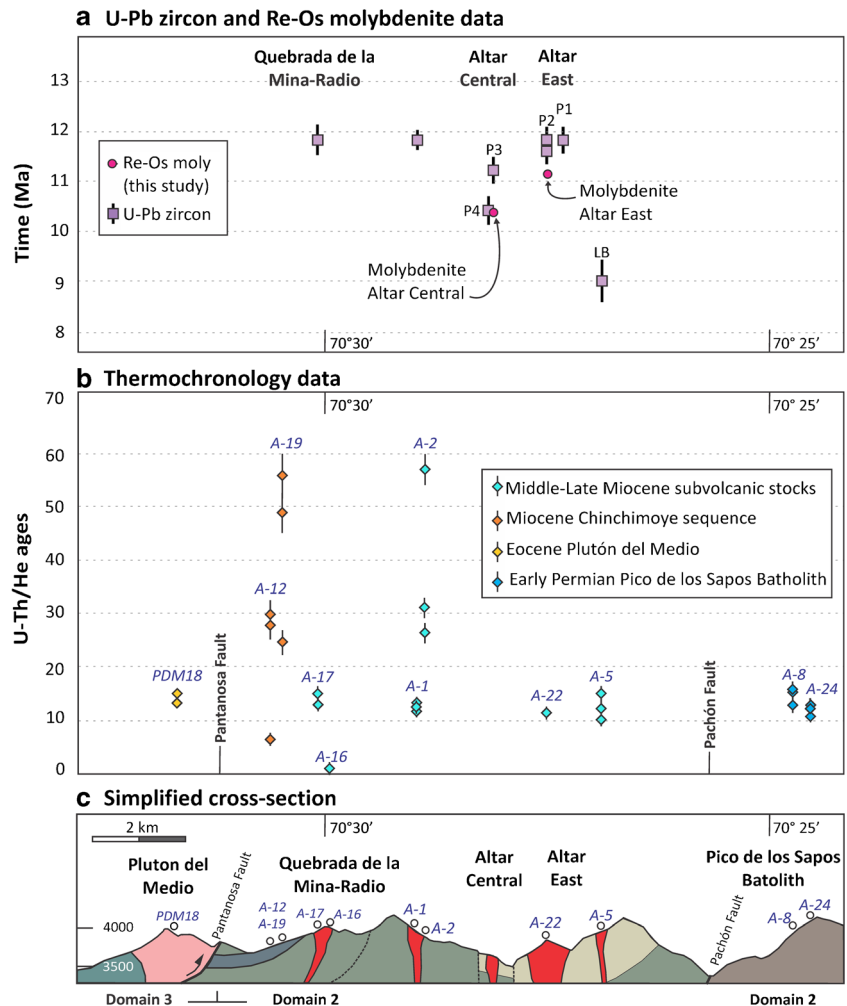


Table 2 Weighted mean U–Th/He ages

Sample	Lithology	Corr age (Ma)	1s ± age (Ma)	Weighted mean age	Error
A-1	Subvolcanic stock	11.53	0.23	12.18	0.15
		12.99	0.27		
		12.28	0.27		
A-2	Subvolcanic stock	30.92	0.97	n.c.	n.c.
		56.83	2.03		
		26.17	1.00		
A-5	Subvolcanic stock	9.96	0.42	12.32	0.26
		14.87	0.42		
		12.00	0.53		
A-24	Pico de Los Sapos Batholith	12.72	0.26	11.87	0.15
		10.66	0.24		
		12.68	0.31		
A-16	Subvolcanic stock	0.82	0.04	0.82	0.04
A-22	Subvolcanic stock	11.17	0.40	11.17	0.40
A-17	Subvolcanic stock	14.87	0.49	13.45	0.27
		12.80	0.33		
		15.69	0.53		
A-8	Pico de Los Sapos Batholith	14.90	0.52	14.3	0.29
		12.71	0.47		
		29.63	1.78		
A-12	Chinchimoye Sequence	27.58	1.66	n.c.	n.c.
		6.15	0.37		
		48.67	2.92		
A-19	Chinchimoye Sequence	55.57	3.33	n.c.	n.c.
		24.44	1.47		
		15.02	0.36		
PDM18	Plutón del Medio	12.98	0.20	13.46	0.17

n.c. not calculated

one apatite crystal from sample A-16 yielded an (U–Th)/He age of $0.82 \text{ Ma} \pm 0.04$ (Table 2).

Discussion

Ages of porphyry emplacement and mineralization

Metallic mineralization at the Altar Central orebody occurred through successive stages of vein formation: (1) quartz ± chalcopyrite ± pyrite veins (A veins) and (2) quartz ± molybdenite veins (B veins), both formed during early potassic alteration at high temperature and pressure, and (3) late stage veins rich in Cu sulfides and sulfosalts (E veins) that formed at low temperature equivalent or transitional to the epithermal environment (Maydagán et al. 2015). In the eastern sector of the Altar deposit, the roots of an epithermal lithocap are exposed, whereas in the central

orebody, epithermal veins cross-cut the porphyry A and B (Maydagán et al. 2015). Fluid inclusion studies have been interpreted to suggest temperatures of 540 to 510 °C and pressures of 1000 to 800 bar for the formation of stage 2 B veins, whereas stage 3 E veins formed, under hydrostatic conditions, from 280 to 250 °C fluids at pressures of 150 to 20 bar (Cioldi 2009; Maydagán et al. 2015).

The two new Re–Os molybdenite dates are interpreted to define the absolute timing of stage 2 B vein mineralization in Altar East ($11.16 \pm 0.06 \text{ Ma}$, Table 1) and Altar Central ($10.38 \pm 0.05 \text{ Ma}$; Table 1) to be Middle Miocene. These ages are nominally different even when including full analytical and decay constant uncertainties (Table 1). As such, although only two ages, the Re–Os molybdenite data suggest that the Altar East and Altar Central deposits were associated with two magmatic hydrothermal centers, as suggested by Maydagán et al. (2014) that were active during two different time periods (Fig. 5a).

Altar East molybdenite (11.16 ± 0.06 Ma) formed a little after the intrusion of Porphyry 2 (11.62 ± 0.21 and 11.68 ± 0.27 Ma) and was contemporaneous, considering uncertainty, with the emplacement of Porphyry 3 (11.13 ± 0.26 Ma). In contrast, the Altar Central molybdenite B veins formed later (10.38 ± 0.05 Ma), at the same time or shortly after the emplacement of Porphyry 4 (10.35 ± 0.32 Ma). The Re–Os ages thus confirm that Altar Central is the youngest magmatic-hydrothermal system in the Altar district.

The mineralization events at Altar can be compared with those from Los Pelambres and El Pachón porphyry deposits, located ~ 25 km south (Fig. 2). Zircon U–Pb crystallization ages of the mineralized porphyries (12.3 to 10.5 Ma) together with the Re–Os molybdenite ages (11.8 to 10.1 Ma) in the Los Pelambres–Frontera system (Bertens et al. 2003, 2006; Perelló

et al. 2012, Fig. 6a) are similar to those of the Altar porphyries and mineralization (Maydagán et al. 2014; this study). Available Re–Os molybdenite ages from El Pachón deposit are, however, younger (9.16 and 8.43 Ma, Bertens et al. 2006, Fig. 6a) and reflect the youngest mineralization event recognized in the Altar–Los Pelambres region (Figs. 2 and 6a).

Cooling and exhumation of the altar district and nearby Los Pelambres–El Pachon deposits

The dispersion of the U–Th/He ages of the Chinchimoye volcanic-sedimentary sequence (samples A-12 and A-19) suggests, at a first glance, that these rocks were not buried sufficiently (< 2 km, depth of the 60 °C isotherm) to reset the U–Th/He system and that the dated apatite still retain, in part, an

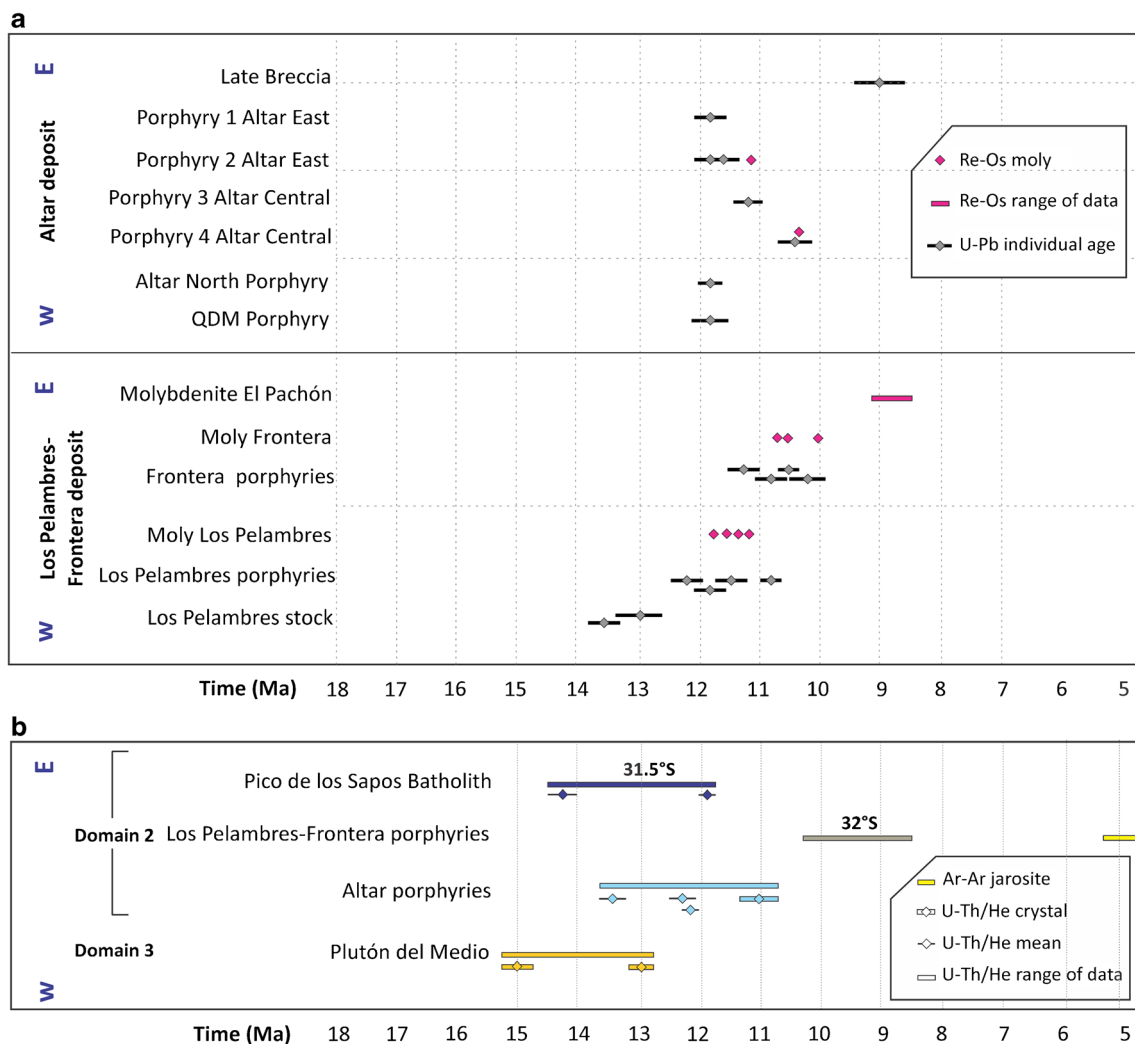


Fig. 6 **a** U–Pb in zircon ages (Maydagán et al. 2011, 2014, 2017) and Re–Os in molybdenite ages from Altar District, comparison with data from Los Pelambres–Frontera and El Pachón deposits (Bertens et al.

2006; Perelló et al. 2012). **b** U–Th/He data from the Altar District, comparison with U–Th/He data from Los Pelambres–Frontera (Perelló et al. 2012) and El Pachón deposits (Bertens et al. 2006)

inherited pre-depositional signal (Fig. 5b). An alternative view for the range in single grain apatite ages is the effect of hydrothermal activity that may influence the thermochronological data sets. However, the sampled sites as well as the volcanic-sedimentary sequence show limited evidence of hydrothermal activity.

The conditions to reset thermochronology systems by late hydrothermal fluids require the fluids to be transported along steeply dipping faults, with a very narrow fracture zone, which results in developing a reset zone that is limited to not more than a few tens of meters around the fault (Luijendijk 2019). The majority of the samples analyzed in this contribution were taken at distance of more than 1–2 km from faults (PDM18, A-12, A-19, A-1, A-2, A-5, A-8, A-24), thus there is no clear evidence to support this hypothesis.

The (U–Th)/He ages obtained in the Altar region, from the Early Permian Pico Los Sapos batholith (LA-ICPMS U–Pb zircon age of 297 Ma, Maydagán 2012) and the Late Eocene Plutón del Medio tonalite (LA-ICPMS U–Pb zircon age of 34.1 Ma, Mpodozis 2016), that range between 15.02 and 10.66 Ma (Table 2; Figs. 3 and 5b, c) reflect a cooling pulse during the Middle Miocene, both in the western sector and in the eastern sector of the Altar deposit. The (U–Th)/He ages of the Permian and Eocene intrusive rocks overlap with the (U–Th)/He dates obtained for the Altar porphyry intrusions (between 14.87 and 9.96 Ma), which also, considering uncertainties, are similar to the U–Pb porphyry crystallization ages (~ 11.9–10.3 Ma, Maydagán et al. 2011, 2014, 2017).

Porphyry deposits occur within magmatic belts worldwide and are spatially, temporally, and genetically related to hypabyssal porphyritic intrusions emplaced at depths between ~ 2 and 6 km (Seedorff et al. 2005; Sillitoe 2010). The intrusions and magma chambers linked to these deposits underwent volatile exsolution and produced a sequence of hydrothermal alteration from ~ 700 to 200 °C (Seedorff et al. 2005; Sillitoe 2010).

The overlap of U–Pb, Re–Os, and (U–Th)/He ages recognized in the Altar subvolcanic stocks, which indicate a very rapid cooling of the magmatic-hydrothermal system, is atypical of low-temperature thermochronology studies on porphyry deposits, where there are generally two distinct cooling periods: magmatic-hydrothermal cooling after emplacement of the intrusion and exhumation cooling (e.g., McInnes et al. 2005; Leng et al. 2018). The overlap in the ages of this study can occur in two ways: (1) the porphyry intrusions are located at very low depths in the crust or (2) a tectonic exhumation event occurs immediately after the emplacement of the intrusion. An example of the first option is the Grasberg porphyry system (Indonesia) in which a depth of emplacement of ~ 0.8 km has been estimated for the intrusion (McInnes et al. 2005). As examples of rapid cooling linked to tectonic

exhumation, we can mention the Middle Eocene dacitic intrusions of the Centinela District (Atacama, Chile), with similar U–Pb and apatite fission track (AFT) ages, that have been interpreted as intruded during the Incaic tectonic phase (Sanchez et al. 2018).

The subvolcanic intrusions of the Altar porphyry deposit were emplaced at depths of 3.5–5 km based on the following evidence: (1) amphibole phenocrysts from porphyry 1 (Altar East) are estimated to have crystallized at 800 °C and pressures between 0.9 and 1.2 kbar that reflect depths of ~ 4 km for pluton emplacement (Maydagán et al. 2014); (2) the early quartz veins have fluid inclusions of intermediate density (Maydagán et al. 2015) that are abundant in samples, 1000 to 600 m below the present surface. The presence of irregular A veins and the fluid inclusions that showed homogenization temperatures between 400 and 540 °C reflect the formation of the veins at lithostatic pressures (Fournier 1999). Exsolution of magmatic volatiles from a crystallizing hydrous magma in the single-phase fluid stability region occur at pressures higher than 1000 bar (e.g., Williams-Jones and Heinrich 2005) equivalent to depths of > 3.5 km at lithostatic pressures; and (3) fluid inclusion studies on B-type veins have been interpreted to indicate pressures of 1000 to 800 bar which correspond to depths of 3.7 to 3 km under lithostatic pressures. In contrast, the telescoping stage 3 epithermal E veins formed, under hydrostatic conditions, from 280 to 250 °C fluids at pressures of 20 to 150 bar that reflect depths of < 2 km (Cioldi 2009; Maydagán et al. 2015).

Considering the temporal data together with the available geological and metallogenetic information of the Altar system, we interpret that the rapid cooling recognized in the Altar intrusions reflects an exhumation pulse that occurred immediately after the emplacement of the subvolcanic intrusion, and that the cooling and related exhumation was contemporaneous with the hypogene mineralization stage of the hydrothermal system.

An alternative interpretation for the (U–Th)/He ages of the subvolcanic stocks sampled close to the porphyry deposit (A-22, A-16, A-17, Fig. 4) would be that the ages indicate the cessation of the hydrothermal activity (< 75 °C). If we consider this hypothesis, it should be noted that more than 50% of the apatite crystals from the subvolcanic stocks have (U–Th)/He ages between 12 and 10 Ma, indicating that the hydrothermal activity of the porphyry and epithermal systems (that are vertically spatial close and are superimposed) would have formed in a short time interval. This provides indirect evidence of uplift, exhumation, and erosion that allowed the porphyry and epithermal systems to be superimposed in a short period of time. Models and field examples of porphyry and lithocap systems in regions without telescoping occur at a vertical distance of ~ 1 km such as the Valeriano lithocap and

associated porphyry copper–gold deposit in northern Chile (Sillitoe 2010; Sillitoe et al. 2016).

Given that (U–Th)/He ages refer to the timing of the closure temperature for He in apatite at ~60–70 °C (Zeitler et al. 1987; Wolf et al. 1998; House et al. 1998; Farley 2002), the (U–Th)/He ages reflect the time when the rocks pass through depths shallower than ~2–3 km. Thus, the U–Pb and (U–Th)/He ages of the porphyry intrusions indicate that the temperature decreased from magmatic crystallization at 800 °C to 60–70 °C in a very short period of time. Given that the majority of the porphyry intrusions in the Altar deposit were emplaced at ~11.75–11.62 Ma and the younger individual (U–Th)/He ages are ~10 Ma, the porphyry intrusions would have been uplifted from its depth of formation at ~4 km to depths shallower than 3 km, and more likely shallower than 2 km based on the epithermal characteristics at Altar Central, in a period of <2 m.y., suggesting high exhumation rates of 0.5–1 km/myr. These exhumation rates are in agreement with a more quantitative estimation (0.4 and 0.6 for a geothermal gradient of 30 °C/km and 0.5 and 0.7 for a geothermal gradient of 20 °C/km) derived by converting the thermochronometric ages into exhumation rates (Willett and Brandon 2013), using the best estimates of the present-day geothermal gradient (Collo et al. 2011; Stevens Goddard and Carrapa 2018).

Lithocaps are large rock volumes, originally 1 to 2 km thick and up to tens of square kilometers in areal extent, that normally constitute the upper parts of porphyry copper systems (Sillitoe 1995). The eastern ridges that surround the Altar east orebody are cut by siliceous ledges that crop out at the surface and have been interpreted to be the basal part of an advanced argillic lithocap (Peregrine Metals Ltd. 2010). A sample of hypogene alunite corresponding to the Altar East lithocap has been dated by Ar–Ar at 12 Ma (Maydagán 2012) reflecting an uplift event after 12 Ma that produced the erosion of the epithermal lithocap and preserved only its roots. The presence of the lithocap remnant would imply at least 1 km of erosion at Altar East and >1 km of erosion at Altar Central.

Further, the similarity of the (U–Th)/He ages at Altar with those of the Permian and Eocene aged plutons indicate that this rapid uplift was not localized to the Altar porphyry–epithermal system, but occurred at a regional scale during the Middle Miocene (14–10 Ma, Fig. 5c). Moreover, the (U–Th)/He zircon and (U–Th)/He ages (10.37 to 8.15 Ma; Bertens et al. 2006, Fig. 6b) recorded in the Los Pelambres deposit, slightly younger than Altar (U–Th)/He ages and very close to the timing of porphyry mineralization (11.66 to 11.00 Ma), coupled with a $^{40}\text{Ar}/^{39}\text{Ar}$ jarosite age (5.34 Ma; Bertens et al. 2006) for supergene alteration, indicate an episode of rapid regional exhumation during the Middle Miocene.

The cooling and interpreted uplift event recorded by the (U–Th)/He ages of the Paleozoic granitoids of the Pico Los Sapos Batholith (14.3 and 11.87 Ma, this study, Fig. 5b, c) coincide with a <14 Ma period of tectonic activity recorded on the Mondaquita Fault (boundary between Domains 1 and 2, Fig. 2) by geological relationships (Mpodozis 2016). South of Río Carnicería, the Mondaquita Fault brings the Mondaca Strata (~22–21 Ma) atop the mid-Miocene volcanic sequence (El Yunque Volcanic Unit, 15–14 Ma; Mpodozis and Cornejo 2012). This geological evidence together with the new thermochronology data suggest that the cooling/exhumation event during porphyry emplacement (Fig. 6b) was linked to uplift/erosion in the Middle to Late Miocene that was associated with faulting between structural Domains 1 and 2 (Fig. 2). The (U–Th)/He ages of the Eocene del Medio Pluton (15.02 and 12.98 Ma) reflect a cooling event and interpreted uplift of structural Domain 3 in the study region (Figs. 5b, c and 6b).

Implications of rapid exhumation and metal endowment

The U–Pb zircon, Re–Os molybdenite, and (U–Th)/He ages show that mineralization at Altar formed penecontemporaneously with the emplacement of porphyry stocks that together were rapidly exhumed. Telescoping of porphyry mineralization and the roots of the high sulfidation epithermal system is more evident in the Altar Central deposit, where epithermal enargite-bearing E veins cross-cut the early potassic alteration stage A and B veins (Zwahlen et al. 2014; Maydagán et al. 2015). Although there are no ages for the sulfides of the epithermal E veins, the superposition of porphyry and epithermal veins, coupled with the U–Pb, Re–Os, and (U–Th)/He ages indicate that exhumation continued during the formation of the Central Altar deposit and permitted the telescoping of porphyry and epithermal mineralization, ultimately enhancing the ore grade at Altar. Based on correlation analysis of assay results and mapped abundances of vein types, approximately 11% to 26% of the copper in the Altar Central orebody is associated with enargite veins, with the bulk of the mineralization being hosted by the early stockwork veining and potassic alteration (Zwahlen et al. 2014). In the Altar Central deposit, this overlap also leads to higher grades in the supergene enrichment zone (Maydagán et al. 2015). In other centers at Altar (e.g., Altar East), this overlap is not so obvious, but veins and disseminations of enargite, bornite, and tennantite with gold locally increase the grades of copper and gold. As such, without the uplift and telescoping, Altar would have been a considerably less economic deposit. This is also likely for many other porphyry systems that have

superimposed epithermal mineralization (e.g., Agua Rica porphyry and Famatina mining district in Argentina, Pudack et al. 2009; Franchini et al. 2011, 2015), show hypogene copper enrichment (e.g., Chuquicamata; Ossandón et al. 2001), or are affected by syn-mineral exhumation (e.g., Los Pelambres deposit, Bertens et al. 2006; Perelló et al. 2012).

Regional tectonic implications and relationships to mineralization

A better understanding of the relationships between tectonism (exhumation/uplift) and copper \pm molybdenum \pm gold mineralization in the Altar–Los Pelambres region requires a broader regional view considering previous regional geochronological and thermochronological studies (Cembrano et al. 2003; Parada et al. 2005, Morata et al. 2010; Ferrando et al. 2014; Lossada et al. 2017, Fig. 7).

The most distinctive geological unit in the central part of the Coastal Range corresponds to the Early Cretaceous Illapel Plutonic Complex (IPC) dated between 118 ± 1.9 and 96 ± 3 Ma (U–Pb zircon and titanite, and $^{39}\text{Ar}/^{40}\text{Ar}$ and K/Ar ages, Morata et al. 2006, 2010; Rivano et al. 1993, Rivano et al. 1985; Ferrando et al. 2014). Further east, in the eastern Coastal Range, Late Cretaceous and Paleocene volcanic sequences are intruded by Paleocene to Eocene granitoids. These include the Late Eocene Fredes–Tres Quebradas pluton (39.1 ± 0.9 , 35.5 ± 0.7 Ma) in the north and the Paleocene Manque Bajo (64.7 ± 1.8 Ma) and Cuncumén plutons (62–59 Ma) in the south (all U–Pb zircon ages; Mpodozis 2016; Rodríguez et al. 2018, Fig. 7).

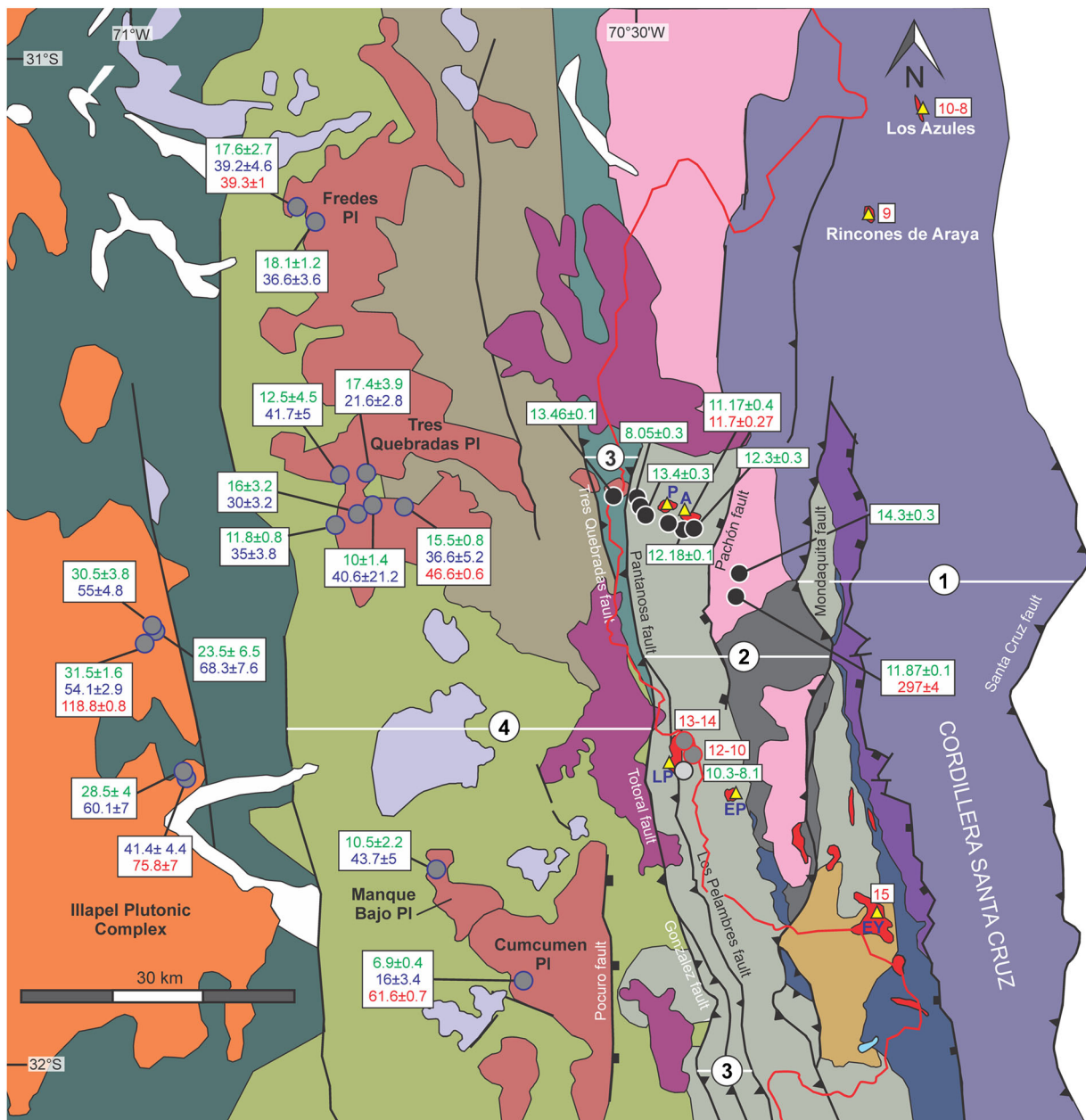
Following crystallization and cooling, the IPC experienced slow cooling and exhumation, as reflected by the AFT ages (68.3 ± 3.8 and 41.4 ± 4.4 Ma; Rodríguez et al. 2018), which show that the IPC crossed the 110 °C isotherm during the Paleocene–Eocene, while (U–Th)/He ages (31.5 ± 1.6 and 23.5 ± 6.5 Ma) indicate that cooling below 70 °C occurred much later, in the Late Oligocene (Rodríguez et al. 2018). In contrast, AFT and (U–Th)/He ages from the Paleocene to Eocene plutons of the eastern Coastal Range (Domain 4) record rapid cooling and uplift events after pluton emplacement. The AFT ages between 41.7 ± 5 and 30 ± 3.2 Ma indicate that the Late Eocene Fredes–Tres Quebradas pluton cooled to the apatite partial annealing zone temperature (125–60 °C) rapidly following emplacement. Further cooling to ≤ 70 °C by the Middle Miocene is evidenced from the 18.1 ± 1.2 to 10 ± 1.4 Ma (U–Th)/He ages (Rodríguez et al. 2018; Fig. 7). A similar cooling path to 125–70 °C and < 70 °C since the Eocene is shown by the AFT (43.7 Ma) and (U–Th)/He (10.5 Ma) ages of the, older, Early Paleocene Manque Bajo stock. However, the data set from the southernmost

Cuncumén pluton (62–59 Ma, Fig. 7) is more difficult to interpret as the AFT (16 Ma) and (U–Th)/He (6.9 Ma) ages (Rodríguez et al. 2018) are younger. This discrepancy is perhaps related to the fact that this intrusive body displays extensive tectonic damage (brecciation, cataclasis) and is located right along the northern termination of the Pucuro Fault, which extends many kilometers to the south along the western slope of the Main Cordillera in the Los Pelambres region (Carter and Aguirre Le-Bert 1965; Rivano and Sepúlveda 1991; Mpodozis et al. 2009, Fig. 7).

Despite this exception, the available data suggest that at the latitude of Altar–Los Pelambres, exhumation and uplift progressed episodically from west to east during the Cretaceous and the Miocene (Rodríguez et al. 2018). The IPC (Fig. 7) probably began to be exhumed as consequence of the onset of Andean compressional deformation in the early Late Cretaceous (Mpodozis and Ramos 1989).

Younger events, recorded further east in the great Altar–Los Pelambres region, include an episode of rapid exhumation in the Late Eocene. This event agrees with the results of thermochronological studies in the Elqui valley, in Chile, at 30°S, that indicate a period of rapid cooling between 35 and 30 Ma (Cembrano et al. 2003; Lossada et al. 2007). This event coincides with the beginning of foredeep sedimentation in Argentina, where sediments derived from the western highlands started to accumulate in the Bermejo foreland basin during the Late Eocene (Fosdick et al. 2017). The rapid cooling/exhumation in the Eocene can be related to the deformation associated with the Incaic Tectonic Event (Steinmann 1929) recognized along the whole Central Andes north of 28°S that was accompanied by the formation of the Bolivian Orocline (Arriagada et al. 2008) and the emplacement of the Late Eocene–Early Oligocene intrusions of the southern Peru–northern Chile porphyry copper province (Sillitoe and Perelló 2005).

The Early Oligocene–Late Oligocene “slow cooling” period observed at 30°S in the Elqui valley region (Lossada et al. 2017) coincides with the intense volcanic activity that gave rise to the Pelambres and Pachón formations and the Mondaca and Río Chicharra Strata which accumulated at the northern end of the Central Chile Abanico/Coya Machalí extensional intra-arc basin (Charrier et al. 2002, 2005; Mpodozis and Cornejo 2012). Volcanism occurred during a period of fast plate convergence rates (Jordan et al. 2001) causing steady westward displacement of the South American Plate (Silver et al. 1998; Kay and Copeland 2006) and weak intraplate coupling (Mpodozis and Cornejo 2012; Horton and Fuentes 2016) when ensuing extensional conditions permitted the production and ascent of large volumes of magmas (Mpodozis and Cornejo 2012; Horton and Fuentes 2016).



Stratified units

- Holocene sedimentary rocks
- Early Miocene volcanic rocks (19-18 Ma)
- Late Oligocene to Early Miocene volcanic rocks
- Paleocene volcanic rocks
- Cretaceous(?) volcanic and sedimentary strata
- Late Cretaceous volcano-sedimentary sequences
- Early to Middle Cretaceous volcano-sedimentary rocks

- Jurassic to Early Cretaceous sedimentary rocks
- Rancho de Lata Formation (Late Triassic)
- Middle Triassic volcanic rocks
- Permo-Triassic Choiyoi volcanic rocks and granitoids

- Paleocene and Eocene intrusive rocks (60-34 Ma)
- Late Cretaceous intrusive rocks (74-65 Ma)
- Early to Middle Cretaceous intrusives
- Early Permian Granitoids

Intrusive units

- Middle to Late Miocene intrusive rocks (15-8 Ma)
- Early Miocene intrusive rocks (24-14 Ma)

Geochronologic data:

- Rodriguez et al. (2018)
- Bertens et al. (2006)
- Perelló et al. (2012)
- This study
- U-Th/He
- FT apatite
- U-Pb
- Thrust faults
- Inverted normal faults
- Lineaments
- Porphyry deposit
- Chile-Argentina boundary

◀ **Fig. 7** Geological map of the Coastal Cordillera, Main Cordillera, and Frontal Cordillera of Chile and Argentina between 31°S and 32°S based on Sernageomin (2003) and Mpodozis (2016). Apatite (U–Th)/He ages are shown together with previous U–Th/He ages and apatite fission track (AFT) ages (Bertens et al. 2006; Rodríguez et al. 2018). U–Pb ages from the Altar region are from Maydagán (2012) and Maydagán et al. (2014). U–Pb ages from Los Pelambres deposit are from Perelló et al. (2012). U–Pb ages from Los Azules, Yunque, and Rincones de Araya deposits are from Zurcher (2008) and Mpodozis and Comejo (2012)

A second period of rapid cooling in the Elqui Valley (30°S, Lössada et al. 2017) in the Early Miocene (ca. 18 Ma) agrees with the 18–15 Ma (U–Th)/He ages obtained in the Domain 4 in the Fredes–Tres Quebradas plutons (Rodríguez et al. 2018, Fig. 7). At this time, there is clear evidence of tectonic activity in the Altar–Pelambres region where field relationships indicate that the Pelambres Fault was active as a thrust fault between 18 and 14 Ma (Mpodozis et al. 2009; Perelló et al. 2012). This event has been also well recognized in Chile and Argentina south of 32°S (Giambiagi et al. 2012; Piquer et al. 2017; Buellow et al. 2018) matching with the beginning of deformation and collapse (inversion) of the extensional Abanico–Coya Machalí Basin (Charrier et al. 2002, 2005; Piquer et al. 2017) and initiation of the shallowing of the subducted Nazca slab, as intraplate coupling between the Nazca and South American Plates increased and convergence rates decreased (Kay and Mpodozis 2002; Mpodozis and Cornejo 2012; Horton and Fuentes 2016).

The younger (U–Th)/He ages obtained at Altar (~15–11 Ma), Los Pelambres, and Pachón (~10–8.1 Ma) indicate very fast, almost instantaneous cooling (and exhumation) during the emplacement of porphyry copper intrusions in Domain 2. Exhumation was again related (and triggered) by active deformation as shown by the post 14 Ma activity documented for the Mondaquita Fault and further east, by the transport of the basement blocks of Santa Cruz and Espinacito ranges of the Frontal Cordillera over the < 18 Ma synorogenic sedimentary strata of the Manantiales foreland basin (Jordan et al. 1996; Pérez 2001; Alarcón and Pinto 2015). Compressional deformation generated crustal shortening through hybrid thin and thick-skinned thrusting (e.g., Cristallini and Ramos 2000; Giambiagi et al. 2003). Crustal thickening during uplift of the Frontal Cordillera and eastward migration of the magmatic front seems to have created the favorable conditions for the generation of water-rich, high Sr/Y “adakitic” magmas at Altar and Los Pelambres (Perelló et al. 2012; Maydagán et al. 2014; Bergoeing 2016) whose presence has been shown to be critical for the formation of most of the porphyry copper deposits around the world (Kay and Mpodozis 2001; Chiaradia et al. 2012; Richards 2011).

Porphyry copper mineralization and deformation at ~ 11–10 Ma coincides with arrival at the trench and beginning of subduction of the E-trending segment of the Juan Fernández Ridge hotspot track below the Los Pelambres–Altar region (Yáñez et al. 2001; Yáñez et al. 2002). Recent studies indicate that the shallowest portion of the flat-slab is associated with the actual inferred location of the subducting Juan Fernández Ridge directly below the Altar–Los Pelambres at 31–32°S (Anderson et al. 2007; Ammiratti et al. 2016). Some authors have proposed a close link between the subduction of aseismic ridges and porphyry copper mineralization (Rosenbaum et al. 2005; Sun et al. 2010). In addition, tectonic perturbations on the downgoing slab could have generated changes in the tectonic stress regime in the crust favorable for magma emplacement and ore formation (Hollings et al. 2005; Maydagán et al. 2011). However, recently, Cu-rich porphyry systems with the same age of 10–11 Ma (Valeriano, Los Helados, Sillitoe and Perelló 2005; Sillitoe et al. 2016) have been discovered along the Chilean–Pampean flat-slab region, up to 400 km north from the Altar–Pelambres, that seem to be located too far north to be directly influenced by the Juan Fernández Ridge subduction. A similar argument can be made for the giant deposits located to the south, where the U–Pb, $^{40}\text{Ar}/^{39}\text{Ar}$, K–Ar, and Re–Os ages of the intrusions related to the copper mineralization, between 6.3 ± 0.1 and 4.3 ± 0.1 Ma at Río Blanco–Los Bronces (Deckart et al. 2014) and between 6.5 ± 0.1 and 4.3 ± 0.1 Ma at El Teniente porphyry deposit (Maksaev et al. 2004; Deckart et al. 2005), seem to be young to be directly linked to the 11–10 Ma subduction of the E-trending Juan Fernández Ridge arm at 31–32°.

If the relationship between Juan Fernández Ridge subduction and generation of fertile copper-enriched magmas is not straightforward, the connection of ridge subduction with rapid cooling, uplift, and exhumation needs to be analyzed. Recent studies have analyzed this relationship in the Pampean flat-slab segment of the Andes (Dávila and Lithgow-Bertelloni 2013; Stevens Goddard and Carrapa 2018). Dávila and Lithgow-Bertelloni (2015) suggested that the collision and subduction of thick aseismic volcanic ridges, like the Juan Fernández Ridge, may drive dynamic uplift in the Andean margin. Examples in other segments of the south American plate are the collision of the Carnegie Ridge in northern Ecuador and the subduction of the Nazca Ridge in southern Peru, where the ridge acted as a wave uplifting the Andean margin as it moved slowly southwards during the Miocene (Wipf et al. 2008; Spikings and Simpson 2014). Another case possibly occurs in the southern Patagonian Andes, where episodic cooling and exhumation results from the subduction of the active Chile Ridge (Ramos 2005; Haschke et al.

2006; Guillaume et al. 2009; Georgieva et al. 2019; Stevens Goddard and Fosdick 2019).

AFT data for Miocene plutons of the Main Andean Range in Chile between 33 and 35°S, south of the location of the subducted E-trending segment of the Juan Fernández Ridge, define a younger and distinct < 10 Ma episode of enhanced crustal cooling through the temperature range of the apatite partial annealing zone (~ 125–60 °C) between 6 and 3 Ma (Maksaev et al. 2009) that cannot be the result of Juan Fernández Ridge subduction. Together with the (U–Th)/He ages for Río Blanco–Los Bronces (3.5 and 2.7 Ma) and El Teniente (3.4 to 2.7 Ma), rapid cooling and exhumation during/after the cessation of igneous and hydrothermal activity occurred at these deposits (McInnes et al. 2005) at a much younger time than at Altar–Los Pelambres. Similar (U–Th)/He ages between 6 and 2 Ma are shown for the Abanico and Farellones formations between 33 and 34°S (Piquer et al. 2017). Also, AFT and (U–Th)/He ages, and numerical models of knickpoint retreat carried out between 33 and 35°S indicate that > 2 km of uplift have occurred since 10.5–4.6 Ma as a consequence of tectonic shortening and “out of sequence” thrusting (Fariás et al. 2008). At these latitudes, to the east, accelerated cooling, rock uplift, and river incision lasting to present day initiated at ~10–9 Ma in the Argentine Frontal Cordillera as a consequence of progressive thrusting of the Frontal Cordillera over the sedimentary fill of the Tunuyán foreland basin (Hilley et al. 2004; Giambiagi et al. 2014; Hoke et al. 2014).

The new data presented here indicate a pulse of rapid cooling/exhumation in the Main Andean Range, at 31–32°, between 15 and 10 Ma. This event was not recorded by Lossada et al. (2017) in the High Andes at 30°S (Elqui Valley) who indicated that only minor erosion, exhumation, and modification of topography has occurred there since the Early Miocene. Slightly older (U–Th)/He ages (18–16 Ma) and similar (U–Th)/He ages (15–10 Ma) were reported by Rodríguez et al. (2018) west of the study area in Chile (Fig. 7). In the Argentine Precordillera and in the foreland, late Miocene and Pliocene cooling ages have been reported (Fosdick et al. 2015; Ortiz et al. 2015; Stevens Goddard and Carrapa 2018).

The Middle–Late Miocene pulse of rapid cooling/exhumation in the study region (15–10 Ma) coincides with tectonic shortening associated with the flattening of the subducted Nazca slab. The youngest (U–Th)/He ages (11–10 Ma) also coincide with the collision of the E-trending arm of the Juan Fernández Ridge with the trench at these latitudes (Yáñez et al. 2001). The ridge subduction seems to be, at least temporally, connected with the pulse of rapid exhumation during the emplacement of the porphyry copper-epithermal deposits in the Main Andean Range at 31–32°S. However, more regional (U–Th)/He dating would be

necessary to determine the extent and distribution of this rapid cooling/exhumation event.

Conclusions

The new (U–Th)/He data presented for El Altar indicate a pulse of rapid cooling/exhumation in the Main Andean Range of Argentina and Chile, at 31°30'S, between 15 and 11 Ma. The (U–Th)/He and Re–Os data presented here, in combination with previous U–Pb geochronology, demonstrate that the exhumation pulse occurred simultaneously with the intrusion of the subvolcanic stocks associated with the Cu–Au mineralization in the Altar deposit, and slightly prior to the exhumation in Los Pelambres deposit. The rapid uplift and exhumation during the formation of the hydrothermal system affected the metal (Cu–Au grades) endowment, by the telescoping of the porphyry system and epithermal mineralization. Without this process the porphyry deposits would have been less economic, with the porphyry system remaining at considerable depth.

This Middle–Late Miocene pulse of exhumation coincides with tectonic shortening associated with the flattening of the subducted Nazca slab and with the collision of the E-trending arm of the Juan Fernández Ridge with the trench, at 11–10 Ma, at this latitude. The ridge subduction seems to be, at least temporally, connected with the pulse of rapid exhumation during the emplacement of the porphyry copper-epithermal deposits in the studied region.

Acknowledgments This work is part of a project funded by Agencia Nacional de Promoción Científica y Tecnológica (ANPCYT): PICT-2016-2689, CONICET (PIP 330), National University of Comahue (PIN 4-I-209), and University of Padova (Progetto di Ateneo 2015, CPDA158355). We express our appreciation to Kevin Heather, John Black, Javier Robeto, Stanford Foy, and Mariano Poodts (Aldebaran Resources) for support to our research studies and to María Isabel Romero, Tadeo Castaño, and all staff of Peregrine Argentina S.A.U. for provision of site access, logistic support, and help during the field work and sampling. D.S. thanks Antonia Hoffman, Geoff Nowell, and Chris Ottley for analytical support, and acknowledges the Total Endowment Fund and CUG Wuhan Dida Fund. Finally, we appreciate the support given by the editor-in-chief Georges Beaudoin, the associated editor Peter Hollings, José Piquer, and an anonymous reviewer for their very helpful comments and reviews.

References

- Aguirre L (1960) Geología de los Andes de Chile Central, Provincia de Aconcagua. Inst Invest Geol 9, Santiago de Chile
- Alarcón P, Pinto L (2015) Neogene erosion of the Andean cordillera in the flat-slab segment as indicated by petrography and whole-rock

- geochemistry from the Manatiales Foreland Basin (32°–32°30'S). *Tectonophysics* 639:1–22
- Aldebaran Resources (2018) Resources Report. <https://www.aldebaranresources.com>. Accessed 28 September 2018
- Alvarez PP (1996) Los depósitos triásicos y jurásicos de la Alta cordillera de San Juan: Geología de la región del Aconcagua provincias de San Juan y Mendoza. *Dir Nac Serv Geol Buenos Aires* 24(5):59–137
- Ammirati JB, Luján SP, Alvarado P, Beck S, Rocher S, Zandt G (2016) High-resolution images above the Pampean flat slab of Argentina (31–32 S) from local receiver functions: implications on regional tectonics. *Earth Planet Sci Lett* 450:29–39
- Anderson M, Alvarado P, Zandt G, Beck S (2007) Geometry and brittle deformation of the subducting Nazca plate, Central Chile and Argentina. *Geophys J Int* 171(1):419–434
- Arriagada C, Roperch P, Mpodozis C, Cobbold PR (2008) Paleogene building of the Bolivian Orocline: tectonic restoration of the Central Andes in 2-D map view. *Tectonics*. <https://doi.org/10.1029/2008TC002269>
- Bergoing JP (2016) Evolución geoquímica del magmatismo de la Región de Los Pelambres (31°S) entre el Cretácico superior y el Mioceno superior: Implicancias para la evolución tectónica y metalogénica de los Andes de Chile Central. Bch Thesis, Departamento de Geología, Universidad de Chile, Santiago, 131 p
- Bertens A, Deckart K, Gonzalez A (2003) Geocronología U–Pb, Re–Os y ^{40}Ar – ^{39}Ar del pórfido de Cu–Mo Los Pelambres, Chile central. *X Congreso Geológico Chileno*, 1 p
- Bertens A, Clark A, Barra F, Deckart K (2006) Evolution of the Los Pelambres–El Pachón porphyry copper–molybdenum district, Chile–Argentina. *XI Congreso Geológico Chileno* 2: 179–181
- Cahill T, Isacks BL (1992) Seismicity and shape of the subducted Nazca plate. *J Geophys Res Solid Earth* 97(B12):17503–17529
- Carter W, Aguirre Le-Bert L (1965) Structural geology of Aconcagua province and its relationship to the central valley graben, Chile. *Geol Soc Am Bull* 76(6):651–664
- Cembrano J, Zentilli M, Grist A, Yáñez G (2003) Nuevas edades de trazas de fisión para Chile Central (30°–34°S): Implicancias en el alzamiento y exhumación de los Andes desde el Cretácico. *X Congreso Geológico Chileno*, 5 p
- Charrier R, Baeza O, Elgueta S, Flynn J, Gans P, Kay SM, Muñoz N, Wyss ZE (2002) Evidence for Cenozoic extensional basin development and tectonic inversion, south of the flat-slab segment, southern Central Andes, Chile (33°–36°). *J S Am Earth Sci* 15:117–139
- Charrier R, Bustamante M, Comte D, Elgueta S, Flynn JJ, Iturra N, Muñoz N, Pardo M, Thiele WAR (2005) The Abanico Extensional Basin: regional extension, chronology of tectonic inversion and relation to shallow seismic activity and Andean uplift. *Neues Jahrb Geol Palaontol Abh* 236:43–77
- Chiaradia M, Ulianov A, Kouzmanov K, Beate B (2012) Why large porphyry Cu deposits like high Sr/Y magmas? *Sci Rep* 2:68
- Cioldi S (2009) The altar exploration project: geology and hydrothermal mineralization paragenesis of the Cu–Mo–Au porphyry deposit, San Juan Province, Argentina, Master thesis, ETH Zurich, 68 p
- Collo G, Dávila FM, Nobile J, Astini RA, Gehrels G (2011) Clay mineralogy and thermal history of the Neogene Vinchina Basin, Central Andes of Argentina: analysis of factors controlling the heating conditions. *Tectonics* 30(4)
- Cooke DR, Hollings P, Walshe JL (2005) Giant porphyry deposits: characteristics, distribution, and tectonic controls. *Econ Geol* 100(5): 801–818
- Cristallini EO, Ramos VA (2000) Thick-skinned and thin-skinned thrusting in the La Ramada fold and thrust belt: crustal evolution of the high Andes of San Juan, Argentina (32 SL). *Tectonophysics* 317(3): 205–235
- Dávila FM, Lithgow-Bertelloni C (2013) Dynamic topography in South America. *J S Am Earth Sci* 43:127–144
- Dávila FM, Lithgow-Bertelloni C (2015) Dynamic uplift during slab flattening. *Earth Planet Sci Lett* 425:34–43
- Deckart K, Clark AH, Aguilar C, Vargas R, Bertens A, Mortensen JK, Fanning M (2005) Magmatic and hydrothermal geochronology of the giant Río Blanco porphyry copper deposit, Central Chile: implications of an integrated U–Pb and ^{40}Ar / ^{39}Ar database. *Econ Geol* 100:905–934
- Deckart K, Silva W, Spröhnle C, Vela I (2014) Timing and duration of hydrothermal activity at the Los Bronces porphyry cluster: an update. *Mineral Deposita* 49(5):535–546
- Fariás M, Charrier R, Carretier R, Martinod J, Fock A, Campbell D, Comte D (2008) Late Miocene high and rapid surface uplift and its erosional response in the Andes of Central Chile (33–35 S). *Tectonics* 27(1)
- Farley KA (2002) (U–Th)/He dating: techniques, calibrations, and applications. *Rev Mineral Geochem* 47:819–844
- Fernández RR, Brown RF, Lencinas AN (1974) Pachón, un nuevo pórfido cuprífero argentino, Departamento de Calingasta, provincia de San Juan, República Argentina. *V Congreso Geológico Argentino* 2:77–89
- Ferrando R, Roperch P, Morata D, Arriagada C, Ruffet G, Córdova ML (2014) A paleomagnetic and magnetic fabric study of the Illapel plutonic complex, coastal range, Central Chile: implications for emplacement mechanism and regional tectonic evolution during the mid-Cretaceous. *J S Am Earth Sci* 50:12–26
- Fillon C, Gautheron C, van der Beek P (2013) Oligocene–Miocene burial and exhumation of the southern Pyrenean foreland quantified by low-temperature thermochronology. *J Geol Soc* 170(1):67–77
- Fosdick JC, Carrapa B, Ortiz G (2015) Faulting and erosion in the Argentine Precordillera during changes in subduction regime: reconciling bedrock cooling and detrital records. *Earth Planet Sci Lett* 432:73–83
- Fosdick JC, Reat EJ, Carrapa B, Ortiz G, Alvarado PM (2017) Retroarc basin reorganization and aridification during Paleogene uplift of the southern Central Andes. *Tectonics* 36(3):493–514
- Fournier RO (1999) Hydrothermal processes related to movement of fluid from plastic into brittle rock in the magmatic-epithermal environment. *Econ Geol* 94(8):1193–1211
- Franchini M, Impiccini A, Lentz D, Ríos J, O'Leary S, Pons J, Schalamuk A (2011) Porphyry to epithermal transition in the Agua Rica polymetallic deposit, Catamarca, Argentina: an integrated petrologic analysis of ore and alteration parageneses. *Ore Geol Rev* 41:49–74
- Franchini M, McFarlane C, Maydagán L, Reich M, Lentz D, Meinert L, Bouhier V (2015) Trace metals in pyrite and marcasite from the Agua Rica porphyry-high sulfidation epithermal deposit, Catamarca, Argentina: textural features and metal zoning at the porphyry to epithermal transition. *Ore Geol Rev* 66:366–387
- Gautheron C, Tassan-Got L (2010) A Monte Carlo approach to diffusion applied to noble gas/helium thermochronology. *Chem Geol* 273(3): 212–224
- Gautheron C, Tassan-Got L, Ketchamand RA, Dobson KJ (2012) Accounting for long alpha-particle stopping distances in (U–Th–Sm)/He geochronology: 3D modeling of diffusion, zoning, implantation, and abrasion. *Geochim Cosmochim Acta* 96:44–56

- Georgieva V, Gallagher K, Sobczyk A, Sobel ER, Schildgen TF, Ehlers TA, Strecker MR (2019) Effects of slab-window, alkaline volcanism, and glaciation on thermochronometer cooling histories, Patagonian Andes. *Earth Pl Sci Lett* 511:164–176
- Giambiagi L, Ramos V, Godoy E, Alvarez PP, Orts S (2003) Cenozoic deformation and tectonic style of the Andes, between 33° and 34° south latitude. *Tectonics* 22(4)
- Giambiagi L, Mescua J, Bechis F, Tassara A, Hoke G (2012) Thrust belts of the southern Central Andes: along strike variations in shortening, topography, crustal geometry and denudation. *Geol Soc Am Bull* 124(7–8):1339–1351
- Giambiagi L, Tassara A, Mescua J, Tunik M, Alvarez PP, Godoy E, Hoke G, Pinto L, Spagnotto S, Poirras H, Tapia F, Jara P, Bechis F, García V, Suriano J, Moreiras SM, Pagano S (2014) Evolution of shallow and deep structures along the Maipo–Tunuyán transect (33° 40' S): from the Pacific coast to the Andean foreland. *Geol Soc London Spec Pub* 399. <https://doi.org/10.1144/SP399.14>
- Guillaume B, Martinod J, Husson L, Roddaz M, Riquelme R (2009) Neogene uplift of central eastern Patagonia: dynamic response to active spreading ridge subduction? *Tectonics* 28(2)
- Haddon A, Porter R (2018) S-wave receiver function analysis of the Pampean flat-slab region: evidence for a torn slab. *Geochim Geophys Geosyst* 19(10):4021–4034
- Haschke M, Sobel ER, Blisniuk P, Strecker MR, Warkus F (2006) Continental response to active ridge subduction. *Geophys Res Lett* 33(15)
- Hilley GE, Strecker MR, Ramos VA (2004) Growth and erosion of fold-and-thrust belts with an application to the Aconcagua fold-and-thrust belt, Argentina. *J Geophys Res Solid Earth* 109(B1)
- Hoke GD, Graber NR, Mescua JF, Giambiagi LB, Fitzgerald PG, Metcalf JR (2014) Near pure surface uplift of the Argentine Frontal Cordillera: insights from (U–Th)/He thermochronometry and geomorphic analysis. *Geol Soc London Spec Pub* 399. <https://doi.org/10.1144/SP399.4>
- Hollings P, Cooke D, Clark A (2005) Regional geochemistry of tertiary igneous rocks in Central Chile: implications for the geodynamic environment of giant porphyry copper and epithermal gold mineralization. *Econ Geol* 100(5):887–904
- Horton BK, Fuentes F (2016) Sedimentary record of plate coupling and decoupling during growth of the Andes. *Geol* 44(8):647–650
- House MA, Wernicke BP, Farley KA (1998) Dating topography of the Sierra Nevada, California, using apatite (U–Th)/He ages. *Nature* 396(6706):66
- Irarrazaval V, Sillitoe RH, Wilson A, Toro JC, Robles W, Lyall G (2010) Discovery history of a giant, high-grade, hypogene porphyry copper molybdenum deposit at Los Sulfatos, Los Bronces–Rio Blanco district, central Chile. *Soc Econ Geol Spec Pub* 15:253–269
- Jordan TE, Tamm V, Figueroa G, Flemings PB, Richards D, Tabbutt K, Cheatham T (1996) Development of the Miocene Manantiales foreland basin, Principal Cordillera, San Juan, Argentina. *Andean Geol* 23(1):43–79
- Jordan TE, Burns WM, Veiga R, Pángaro F, Copeland P, Kelley S, Mpodozis C (2001) Extension and basin formation in the southern Andes caused by increased convergence rate: a mid-Cenozoic trigger for the Andes. *Tectonics* 20(3):308–324
- Kay SM, Copeland P (2006) Early to middle Miocene back-arc magmas of the Neuquén basin of the southern Andes: geochemical consequences of slab shallowing and the westward drift of South America (35°–39° S lat.). *Geol Soc Am Spec Paper* 40:185–213
- Kay SM, Mpodozis C (2001) Central Andean ore deposits linked to evolving shallow subduction systems and thickening crust. *GSA Today* 11:4–9
- Kay SM, Mpodozis C (2002) Magmatism as a probe to the Neogene shallowing of the Nazca plate beneath the modern Chilean flat-slab. *J S Am Earth Sci* 15:39–57
- Klohn C (1960) Geología de la Cordillera de los Andes de Chile Central, provincias de Santiago, O'Higgins, Colchagua y Curicó. *Inst Invest Geol (Chile)* 8:95
- Kraml M, Pik R, Rahn M, Selbekk R, Carignan J, Keller J (2006) A new multi-mineral age reference material for $^{40}\text{Ar}/^{39}\text{Ar}$, (U–Th)/He and fission track dating methods: the Limberg t3 tuff. *Geostand Geoanal Res* 30(2):73–86
- Lencinas A, Tonel M (1993) La Brecha Sur del Yacimiento de Cobre Porfídico de Pachón, San Juan, República Argentina. *XI Congreso Geológico Argentino* pp:241–247
- Li Y, Selby D, Feely M, Costanzo A, Li XH (2017) Fluid inclusion characteristics and molybdenite Re–Os geochronology of the Qulong porphyry copper–molybdenum deposit, Tibet. *Mineral Deposita* 52(2):137–158
- Lossada AC, Giambiagi L, Hoke GD, Fitzgerald PG, Creixell C, Murillo I, Suriano J (2017) Thermochronologic evidence for late Eocene Andean mountain building at 30° S. *Tectonics* 36(11):2693–2713
- Luijendijk E (2019) Beo v1.0: numerical model of heat flow and low-temperature thermochronology in hydrothermal systems. *Geosci Model Dev*. <https://doi.org/10.5194/gmd-2018-341>
- Mackaman-Lofland C, Horton BK, Fuentes F, Constenius KN, Stockli DF (2019) Mesozoic to Cenozoic retroarc basin evolution during changes in tectonic regime, southern Central Andes (31–33°S): insights from zircon U–Pb geochronology. *J S Am Earth Sci* 89:299–318
- Maksaev V, Munizaga F, McWilliams M, Fanning M, Mathur R, Ruiz J, Zentilli M (2004) New chronology for El Teniente, Chilean Andes, from U/Pb, $^{40}\text{Ar}/^{39}\text{Ar}$, Re–Os and fission track dating: implications for the evolution of a supergiant porphyry Cu–Mo deposit. *Soc Econ Geol Spec Pub* 11:15–54
- Maksaev V, Munizaga F, Zentilli M, Charrier R (2009) Fission track thermochronology of Neogene plutons in the principal Andean cordillera of Central Chile (33–35° S): implications for tectonic evolution and porphyry Cu–Mo mineralization. *Andean Geol* 36(2):153–171
- Maydagán L (2012) El Prospecto de Cu–(Au–Mo) Altar (31° 29'LS, 70° 28'LO), San Juan: Unpublished PhD thesis, Bahía Blanca, Argentina, Universidad Nacional del Sur, 340 p
- Maydagán L, Franchini M, Chiaradia M, Pons J, Impiccini A, Toohey J, Rey R (2011) Petrology of the Miocene igneous rocks in the Altar region, main Cordillera of San Juan, Argentina. A geodynamic model within the context of the Andean flat-slab segment and metallogenesis. *J S Am Earth Sci* 32(1):30–48
- Maydagán L, Franchini M, Chiaradia M, Dilles J, Rey R (2014) The altar porphyry Cu–(Au–Mo) deposit (Argentina): a complex magmatic-hydrothermal system with evidence of recharge processes. *Econ Geol* 109(3):621–641
- Maydagán L, Franchini M, Rusk B, Lentz DR, McFarlane C, Impiccini A, Ríos J, Rey R (2015) Porphyry to epithermal transition in the Altar Cu–(Au–Mo) deposit, Argentina, studied by cathodoluminescence, LA-ICP-MS, and fluid inclusion analysis. *Econ Geol* 110(4):889–923
- Maydagán L, Franchini M, Chiaradia M, Bouhier V, Di Giuseppe N, Rey R, Dimieri L (2017) Petrogenesis of Quebrada de la Mina and Altar north porphyries (Cordillera of San Juan, Argentina): crustal assimilation and metallogenic implications. *Geosci Front* 8(5):1135–1159
- McDowell FW, McIntosh WC, Farley KA (2005) A precise ^{40}Ar – ^{39}Ar reference age for the Durango apatite (U–Th)/He and fission-track dating standard. *Chem Geol* 214(3–4):249–263

- McInnes BIA, Evans NJ, Fu FQ, Garwin S, Belousova E, Griffin WL, Bertens A, Sukarna D, Permanadewi S, Andrew R, Deckart K (2005) Thermal history analysis of selected Chilean, Indonesian and Iranian porphyry Cu–Mo–Au deposits. In: Porter TM (ed) Super porphyry copper and gold deposits: a global perspective. Porter Geoconsultancy Publishing, Adelaide, pp 27–42
- Morata D, Féraud G, Schärer U, Aguirre L, Belmar M, Cosca M (2006) A new geochronological framework for lower Cretaceous magmatism in the coastal range of Central Chile. XI Congreso Geológico Chileno, 2 p
- Morata D, Varas MJ, Higgins M, Valencia V, Verhoort J (2010) Episodic emplacement of the Illapel Plutonic Complex (Coastal Cordillera, Central Chile): Sr and Nd isotopic, and zircon U–Pb geochronological constraints. South American Symposium on Isotope Geology 7: 1300169–1300167
- Mpodozis C (2016) Mapa Geológico Regional del Área de Los Pelambres (escala 1:75.000). Informe Interno, Antofagasta Minerals, Santiago, Chile
- Mpodozis C, Cornejo P (2012) Cenozoic tectonics and porphyry copper systems of the Chilean Andes. Soc Econ Geol Spec Pub 16:329–360
- Mpodozis C, Kay SM (1992) Late Paleozoic to Triassic evolution of the Gondwana margin: evidence from Chilean frontal cordilleran batholiths (28° S to 31° S). Geol Soc Am Bull 104(8):999–1014
- Mpodozis C, Ramos VA (1989) The Andes of Chile and Argentina. In: Erickson GE, Cañas MT, Reinemund JA (eds) Geology of the Andes and its relation to hydrocarbon and mineral resources. Circum-Pacific Council for Energy and Mineral Resources, earth Sci series, vol 11, pp 59–90
- Mpodozis C, Rivano S, Parada MA, Vicente JC (1976) Acerca del plutonismo tardi-hercínico en la Cordillera Frontal entre los 30° y 33° sur (Provincia de Mendoza y San Juan, Argentina). V Congreso Geológico Argentino, Bahía Blanca, pp 143–71
- Mpodozis C, Brockway H, Marquardt C, Perelló J (2009) Geocronología U/Pb y tectónica de la región de Los Pelambres–Cerro Mercedario: Implicancias para la evolución cenozoica de los Andes del centro de Chile y Argentina. XII Congreso Geológico Chileno: S9, 4 p–S059
- Musso RJE, Pérez DJ, Rey R, Toohey J (2012) Geología de las nacientes del río La Pantanosa, Cordillera Frontal (31°3'S), Provincia de San Juan, Argentina, Congreso Geológico Chileno, Santiago, pp 250–251
- Mutschler FE, Ludington S, Bookstrom AA (2010) Giant porphyry related metal camps of the world—a database: USGS open-file report 99-556, Online Version 1.0, <http://pubs.usgs.gov/of/1999/of99-556>. Accessed 9 March 2010
- Ortiz G, Alvarado P, Fosdick JC, Perucca L, Saez M, Venerdini A (2015) Active deformation in the northern sierra de Valle Fértil, sierras Pampeanas, Argentina. J S Am Earth Sci 64:339–350
- Ossandón CG, Fréraud CR, Gustafson LB, Lindsay DD, Zentilli M (2001) Geology of the Chuquicamata mine: a progress report. Econ Geol 96(2):249–270
- Parada MA, Féraud G, Fuentes F, Aguirre L, Morata D, Larrondo P (2005) Ages and cooling history of the early Cretaceous Caleu pluton: testimony of a switch from a rifted to a compressional continental margin in Central Chile. J Geol Soc 162(2):273–287
- Peregrine Metals Ltd (2010) Altar project San Juan province Argentina: NI 43-101 Technical Report, 159 p
- Perelló J, Sillitoe RH, Mpodozis C, Brockway H, Posso H (2012) Geologic setting and evolution of the porphyry copper–molybdenum and copper–gold deposits at Los Pelambres, Central Chile. Soc Econ Geol Spec Pub 16:79–104
- Pérez DJ (2001) Tectonic and unroofing history of Neogene Manantiales foreland basin deposits, Cordillera Frontal (32°30'S), San Juan Province, Argentina. J S Am Earth Sci 14:693–705
- Piquer J, Hollings P, Rivera O, Cooke DR, Baker M, Testa F (2017) Along-strike segmentation of the Abanico Basin, Central Chile: new chronological, geochemical and structural constraints. Lithos 268:174–197
- Pudack C, Halter WE, Heinrich CA, Pettke T (2009) Evolution of magmatic vapor to gold-rich epithermal liquid: the porphyry to epithermal transition at Nevados de Famatina, Northwest Argentina. Econ Geol 104(4):449–477
- Ramos VA (2005) Seismic ridge subduction and topography: foreland deformation in the Patagonian Andes. Tectonophysics 399(1–4):73–86
- Ramos VA, Jordan TE, Allmendinger RW, Mpodozis C, Kay SM, Cortés JM, Palma M (1986) Paleozoic terranes of the central Argentine–Chilean Andes. Tectonics 5(6):855–880
- Richards JP (2011) High Sr/Y arc magmas and porphyry Cu–Mo–Au deposits: just add water. Econ Geol 106:1075–1081
- Rivano S, Sepúlveda P (1991) Hoja Illapel (1:250.000) Región de Coquimbo. Servicio Nacional de Geología y Minería. Carta Geol Chile 69:1–132
- Rivano S, Sepúlveda P, Hervé F, Godoy E (1985) Geocronología K–Ar de las rocas intrusivas entre los 31–32° S, Chile. Rev Geol Chile 24: 63–64
- Rivano S, Sepúlveda P, Boric R, Espiñeira P (1993) Mapa Geológico de la Hoja Quillota-Portillo (escala 1:250.000), V Región de Valparaíso. Carta Geol Chile 73
- Rodríguez MP, Charrier R, Bricchau S, Carretier S, Fariás M, de Parseval P, Ketcham RA (2018) Latitudinal and longitudinal patterns of exhumation in the Andes of North-Central Chile. Tectonics 37(9): 2863–2886
- Rosenbaum G, Giles D, Saxon M, Betts PG, Weinberg R, Duboz C (2005) Subduction of the Nazca Ridge and the Inca Plateau: insights into the formation of ore deposits in Peru. Earth Planet Sci Lett 239: 18–32
- Sanchez C, Bricchau S, Riquelme R, Carretier S, Bissig T, Lopez C, Mpodozis C, Campos E, Regard V, Héral G, Marquardt C (2018) Exhumation history and timing of supergene copper mineralisation in an arid climate: new thermochronological data from the Centinela District, Atacama, Chile. Terra Nova 30(1):78–85
- Sato AM, Llambias EJ, Basei MA, Castro CE (2015) Three stages in the late Paleozoic to Triassic magmatism of southwestern Gondwana, and the relationships with the volcanogenic events in coeval basins. J S Am Earth Sci 63:48–69
- Seedorff E, Dilles JH, Proffett JM, Einaudi MT, Zurcher L, Stavast WJA, Johnson D, Barton MD (2005) Porphyry deposits: characteristics and origin of hypogene features. Econ Geol 100:251–298
- Selby D, Creaser RA (2004) Macroscale NTIMS and microscale LA-MC-ICP-MS Re–Os isotopic analysis of molybdenite: testing spatial restrictions for reliable Re–Os age determinations, and implications for the decoupling of Re and Os within molybdenite. Geochim Cosmochim Acta 68(19):3897–3908
- Sernageomin (2003) Mapa Geológico de Chile: versión digital. Servicio Nacional de Geología y Minería, Publicación Geológica Digital, No. 4 CD-Room
- Sillitoe RH (1994) Erosion and collapse of volcanoes: causes of telescoping in intrusion-centered ore deposits. Geology 22(10):945–948
- Sillitoe RH (1995) Exploration and discovery of base- and precious-metal deposits in the circum-Pacific region during the last 25 years. Resour Geol 19
- Sillitoe RH (2010) Porphyry copper systems. Econ Geol 105(1):3–41
- Sillitoe RH, Perelló J (2005) Andean copper province: tectonomagmatic settings, deposit types, metallogeny, exploration, and discovery. Econ Geol 100:845–890
- Sillitoe RH, Burgoa C, Hopper D (2016) Porphyry copper discovery beneath the Valeriano lithocap, Chile. SEG News 106:15–20

- Sillitoe RH, Devine FA, Sanguinetti MI, Friedman RM (2019) Geology of the Josemaría porphyry copper–gold deposit, Argentina: formation, exhumation, and burial in two million years. *Econ Geol* 114(3): 407–426
- Silver PG, Russo RM, Lithgow-Bertelloni C (1998) Coupling of South American and African plate motion and plate deformation. *Science* 279(5347):60–63
- Spikings R, Simpson G (2014) Rock uplift and exhumation of continental margins by the collision, accretion, and subduction of buoyant and topographically prominent oceanic crust. *Tectonics* 33(5):635–655
- Steinmann G (1929) *Geologie von Peru*. C. Winter, Heidelberg, vol. 460
- Stevens Goddard AL, Carrapa B (2018) Using basin thermal history to evaluate the role of Miocene–Pliocene flat-slab subduction in the southern Central Andes (27 S–30 S). *Basin Res* 30(3):564–585
- Stevens Goddard AL, Fosdick JC (2019) Multichronometer thermochronologic modelling of migrating spreading ridge subduction in southern Patagonia. *Geology* 47:555–558
- Sun W, Ling M, Yang X, Fan W, Ding X, Liang H (2010) Ridge subduction and porphyry copper–gold mineralization: an overview. *Sci China Earth Sci* 53(4):475–484
- Thiele R (1980) Hoja Santiago, Región Metropolitana. Servicio Nacional de Geología y Minería. *Carta Geol Chile*, Chile (29) 21
- Willett SD, Brandon MT (2013) Some analytical methods for converting thermochronometric age to erosion rate. *Geochem Geophys Geosyst* 14(1):209–222
- Williams-Jones AE, Heinrich CA (2005) 100th anniversary special paper: vapor transport of metals and the formation of magmatic-hydrothermal ore deposits. *Econ Geol* 100(7):1287–1312
- Wipf M, Zeilinger G, Seward D, Schlunegger F (2008) Focused subaerial erosion during ridge subduction: impact on the geomorphology in South-Central Peru. *Terra Nova* 20:1–10
- Wolf RA, Farley KA, Kass DM (1998) Modeling of the temperature sensitivity of the apatite (U–Th)/He thermochronometer. *Chem Geol* 148(1–2):105–114
- Yáñez G, Ranero CR, von Huene R, Díaz J (2001) Magnetic anomaly interpretation across the southern Central Andes (32°–34°S): the role of the Juan Fernández ridge in the late Tertiary evolution of the margin. *J Geophys Res* 106:6325–6345
- Yáñez G, Cembrano J, Pardo M, Ranero C, Selles D (2002) The Challenger–Juan Fernández–Maipo major tectonic transition of the Nazca–Andean subduction system at 33–34 S: geodynamic evidence and implications. *J S Am Earth Sci* 15(1):23–38
- Zeitler PK, Herczeg AL, McDougall I, Honda M (1987) U–Th–He dating of apatite: a potential thermochronometer. *Geochim Cosmochim Acta* 51(10):2865–2868
- Zurcher L (2008) U–Pb geochronology of rocks from the Los Azules porphyry deposit, San Juan, Argentina. *Minera Andes, Inc. progress report*, Tucson, Arizona, 8 p
- Zwahlen C, Cioldi S, Wagner T, Rey R, Heinrich C (2014) The porphyry Cu–(Mo–Au) deposit at Altar (Argentina): tracing gold distribution by vein mapping and LA-ICP-MS mineral analysis. *Econ Geol* 109(5):1341–1358

Publisher's note Springer Nature remains neutral with regard to jurisdictional claims in published maps and institutional affiliations.